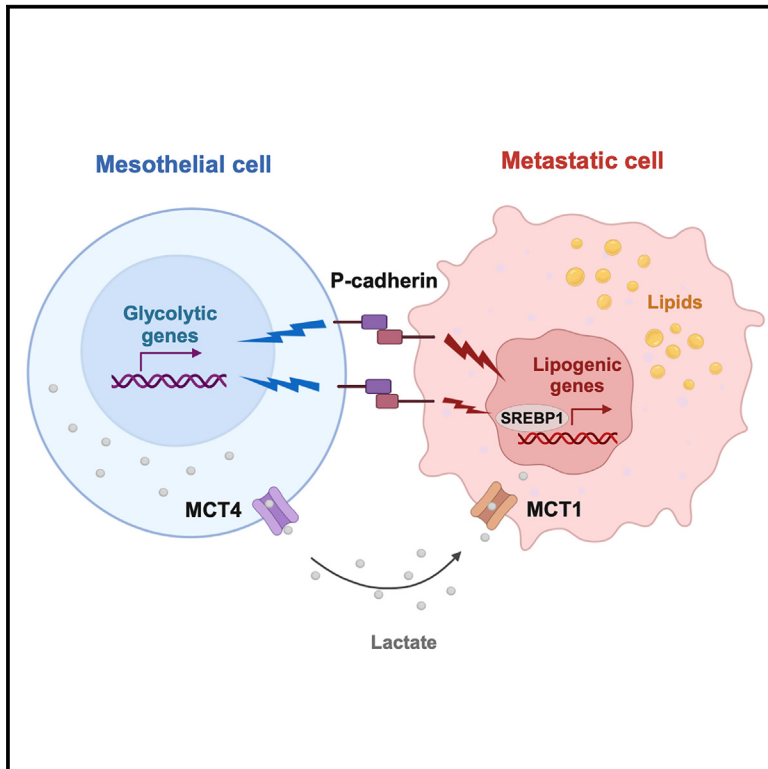# P-cadherin mechanoactivates tumor-mesothelium metabolic coupling to promote ovarian cancer metastasis

Graphical abstract

Authors

Jing Ma, Sally Kit Yan To,
Katie Sze Wai Fung, ..., Hong-Yan Guo,
Chi Bun Chan, Alice Sze Tsai Wong

Correspondence

chancb@hku.hk (C.B.C.),
awong1@hku.hk (A.S.T.W.)

In brief

Ma et al. demonstrate that heterotypic P-cadherin interactions can transduce distinct mechanical signals between metastatic cancer cells and the interacting tumor mesothelium. This interaction facilitates a lipogenic-glycolytic metabolic coupling between the two cell types, thereby reinforcing peritoneal metastasis in ovarian cancer.

Highlights

- P-cadherin mediates adhesion of metastatic ovarian cancer cells to the mesothelium

- P-cadherin binding mechanically stimulates glycolysis in the mesothelium, producing lactate

- Lactate is shuttled into metastatic cells to support *de novo* lipogenesis via SREBP1

- Targeting P-cadherin-mediated metabolic coupling may limit peritoneal metastasis

CellPress

Cell Reports

Article

P-cadherin mechanoactivates tumor-mesothelium metabolic coupling to promote ovarian cancer metastasis

Jing Ma,[1,2,9] Sally Kit Yan To,[1,3,9] Katie Sze Wai Fung,[1,3,9] Kun Wang,[1,9] Jiangwen Zhang,[1] Alfonso Hing Wan Ngan,[4] Susan Yung,[5] Tak Mao Chan,[5] Carmen Chak Lui Wong,[6] Philip Pun Ching Ip,[6] Ling Peng,[7] Hong-Yan Guo,[8] Chi Bun Chan,[1,*] and Alice Sze Tsai Wong[1,10,*]

[1]School of Biological Sciences, University of Hong Kong, Pokfulam Road, Hong Kong, China
[2]Department of Pharmacy, South China Hospital, Medical School, Shenzhen University, Shenzhen 518116, China
[3]Laboratory for Synthetic Chemistry and Chemical Biology Limited, 17W, Hong Kong Science and Technology Parks, New Territories, Hong Kong, China
[4]Department of Mechanical Engineering, University of Hong Kong, Pokfulam Road, Hong Kong, China
[5]Department of Medicine, School of Clinical Medicine, University of Hong Kong, Queen Mary Hospital, Sassoon Road, Hong Kong, China
[6]Department of Pathology, School of Clinical Medicine, University of Hong Kong, Queen Mary Hospital, Sassoon Road, Hong Kong, China
[7]Aix-Marseille Université, CNRS, Centre Interdisciplinaire de Nanoscience de Marseille, UMR, 13288 Marseille, France
[8]Department of Obstetrics and Gynecology, Peking University Third Hospital, Beijing 100191, China
[9]These authors contributed equally
[10]Lead contact
*Correspondence: chancb@hku.hk (C.B.C.), awong1@hku.hk (A.S.T.W.)
https://doi.org/10.1016/j.celrep.2024.115096

SUMMARY

Cancer adhesion to the mesothelium is critical for peritoneal metastasis, but how metastatic cells adapt to the biomechanical microenvironment remains unclear. Our study demonstrates that highly metastatic (HM), but not non-metastatic, ovarian cancer cells selectively activate the peritoneal mesothelium. HM cells exert a stronger adhesive force on mesothelial cells via P-cadherin, an adhesion molecule abundant in late-stage tumors. Mechanical activation of P-cadherin enhances lipogenic gene expression and lipid content in HM cells through SREBP1. P-cadherin also induces glycolysis in the interacting mesothelium without affecting lipogenic activity, with the resulting lactate serving as a substrate for lipogenesis in HM cells. Nano-delivery of small interfering RNA (siRNA) targeting P-cadherin or MCT1/4 transporters significantly suppresses metastasis in mice. Moreover, increased fatty acid synthase levels in metastatic patient samples correlate with high P-cadherin expression, supporting enhanced *de novo* lipogenesis in the metastatic niche. This study reveals P-cadherin-mediated mechano-metabolic coupling as a promising target to restrain metastasis.

INTRODUCTION

Ovarian cancer is the leading cause of mortality among gynecological malignancies. Metastatic ovarian cancer cells exhibit a marked predilection for colonizing the peritoneum and omentum.[1,2] Peritoneal metastasis, although less frequent than blood-borne metastasis, poses significant challenges for treatment due to its rapid and extensive dissemination fueled by positive feedback mechanisms. The aggressive nature of this dissemination mode renders current therapies largely ineffective, resulting in a 5-year survival rate of less than 25% for individuals with advanced-stage disease.[3]

Metastasis is a complex and highly inefficient process, with less than 0.01% of disseminated cancer cells successfully establishing themselves in a target tissue and initiating new metastatic growth.[4] In the context of peritoneal metastasis, adhesion to the mesothelium lining at the peritoneal surface is a first critical step.[5] Mesothelial cells were traditionally considered passive barriers, but emerging research indicates their active involvement in shaping the metastatic microenvironment in ovarian cancer. Studies have shown that cancer-associated mesothelial cells could secrete extracellular matrix proteins such as fibronectin and collagen, cytokines and chemokines like interleukin (IL)-8 and CCL2, as well as soluble proteins such as angiopoietin-like 4 and osteopontin, which may collectively create a favorable environment that promotes tumor adhesion, chemoresistance, and immune evasion.[6–11] On the other hand, metastatic cancer cells have been found to induce mesenchymal transition in mesothelial cells via IL-1 and transforming growth factor β.[8,10] However, since these studies have primarily focused on secreted factors, the involvement of cell-cell contact in signal transduction remains largely unknown.

Metastatic cells possess remarkable capability to sense and respond to a wide range of biochemical and biophysical signals
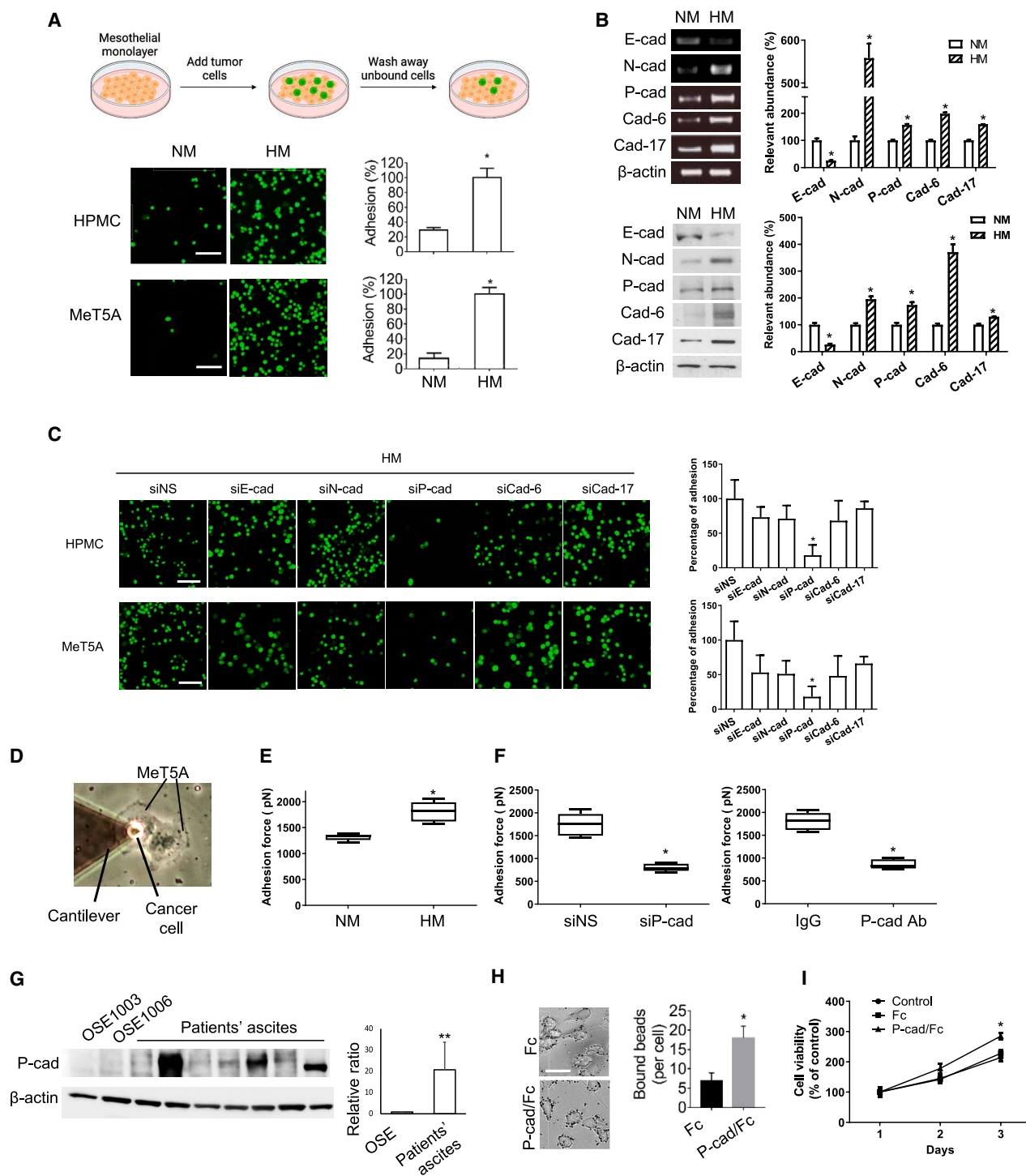
Figure 1. P-cadherin mechanically modulates tumor-mesothelial adhesion

(A) Adhesion assays were performed to evaluate the adhesive capabilities of non-metastatic (NM) and highly metastatic (HM) cells (labeled green with the green-fluorescent chloromethyl derivatives of fluorescein diacetate [CMFDA] dye) to confluent monolayers of human peritoneal mesothelial cells (HPMCs) or MeT5A cells. Representative fluorescent images and quantification of adhered cells are shown. Scale bar, 100 μm.

(B) Expression levels of P-cadherin (P-cad), E-cadherin (E-cad), N-cadherin (N-cad), cadherin-6 (Cad-6), and cadherin-17 (Cad-17) in NM and HM cells were analyzed by RT-PCR and western blot.

(C) Mesothelial adhesion assays were performed with HM cells transfected with non-specific (NS), E-cad, N-cad, P-cad, Cad-6, or Cad-17 siRNA (green). Representative fluorescent images and quantification of adhered cells are shown. Scale bar, 100 μm.

(legend continued on next page)

from their surrounding microenvironment. Although the biomechanics of tumor microenvironment, known as the mechano-niche, have long been overlooked, they are now recognized as distinct features in cancer development and progression.[12,13] Mechanosensitive proteins have emerged as promising and unique targets for cancer therapeutics. The mechano-niche encompasses various factors, such as tissue stiffness, extracellular matrix composition, and mechanical forces, that can profoundly influence the behaviors and functions of cancer cells. In addition to adapting to the dynamic mechanical changes, metastatic cells must also meet diverse metabolic demands during their journey. Significant rewiring of metabolic circuits, including aerobic glycolysis, oxidative phosphorylation, lipid metabolism, and glutamine metabolism, is regarded as a hallmark of cancer. However, the precise mechanisms by which the mechano-niche impacts cancer cell metabolism remain largely unknown.

Cadherins are well-known mechanosensitive sensors that transmit both outside-in and inside-out signals that modulate their conformation and adhesive properties.[14,15] E-cadherin-mediated mechanotransduction was shown to regulate glucose uptake through the activation of adenosine monophosphate-activated protein kinase (AMPK),[16] while another study reported that heterophilic E-cadherin/N-cadherin mechanical signaling could drive collective migration.[17] Despite these findings, the functional significance and molecular mechanisms of mechanical signaling by cadherins are largely unexplored. Our present study aims to investigate the potential role of cadherin in establishing a connection between cell adhesion mechanics and metabolic reprogramming at the mesothelial metastatic niche. Our results reveal the role of P-cadherin, distinguishing it from other cadherins, in activating the peritoneal niche and establishing metabolic coupling with the mesothelium during peritoneal colonization. These significant findings underscore the therapeutic potential of targeting P-cadherin-mediated mechanotransduction for the treatment of peritoneal metastasis.

RESULTS

P-cadherin promotes the adhesion of metastatic cells to the mesothelium

To elucidate the molecular basis of metastasis under tightly controlled conditions, we have established an isogenic model of spontaneous human ovarian cancer metastasis consisting of the highly metastatic (HM)-non-metastatic (NM) cell pair.[18,19] Orthotopic injection in both immunocompromised and humanized mouse models revealed that HM cells rapidly metastasized within the peritoneum, closely mirroring human ovarian cancer dissemination patterns, whereas NM cells did not metastasize despite exhibiting similar tumorigenicity as HM cells.[18,19] To ensure that our observations were not cell-line specific, we

have used HM-NM pairs derived from HEYA8 and OVSAHO cell lines. To mimic tumor-mesothelial interaction, we conducted mesothelial adhesion assays. Both primary human peritoneal mesothelial cells (HPMCs) and human mesothelial cell line MeT5A were employed to ensure the robustness of our observations. A significant increase in the adhesion of HEYA8 HM cells to mesothelial cell monolayer compared to their NM counterparts was observed (HPMC, 3.40 ± 0.25-fold increase; MeT5A, 7.14 ± 0.64-fold increase; Figure 1A). Similar results were obtained when using the OVSAHO HM-NM cell pair (4.54 ± 0.40-fold increase; Figure S1A), indicating that metastatic cells are more capable of adhering to the mesothelium. Conditioned medium from either HM or MeT5A cells alone did not affect HM-MeT5A adhesion (Figure S1B), further suggesting the involvement of a contact-dependent mechanism in this tumor-mesothelium interaction.

To identify the cell adhesion molecule responsible for mediating the interaction between HM cells and the mesothelium, we examined the expression of E-cadherin, N-cadherin, P-cadherin, cadherin-6, and cadherin-17, which have previously been implicated in the progression of ovarian cancer.[20–22] Our analysis showed significantly lower expression of E-cadherin and significantly higher expression of the other cadherins at both the mRNA and protein levels in HEYA8 HM cells compared to NM cells (Figure 1B). Similar protein expression changes were observed in OVSAHO cell pair (Figure S1C). To identify which of these cadherins is important for the interaction, we used corresponding small interfering RNAs (siRNAs) to target E-cadherin (siE-cad), N-cadherin (siN-cad), P-cadherin (siP-cad), cadherin-6 (siCad-6), and cadherin-17 (siCad-17). We found that specifically blocking P-cadherin resulted in a significant decrease in the mesothelial adhesion of HEYA8 HM cells. The adhesion of HEYA8 HM to HPMC or MeT5A decreased notably with siP-cad (83% ± 7%), whereas siE-cad (27% ± 15%), siN-cad (29% ± 19%), siCad-6 (36% ± 9%), and siCad-17 (10% ± 10%) did not exhibit significant reductions compared to a non-specific siRNA (siNS) control (Figure 1C). All siRNA showed similar knockdown efficiency (Figure S1D). Additionally, siP-cad significantly reduced adhesion of OVSAHO HM cells (HPMC 68% ± 11% and MeT5A 77% ± 8%) (Figure S1E). The expression of P-cadherin was detected in both HPMC and MeT5A (Figure S1F). These data together support the specific involvement of P-cadherin during HM-MeT5A interactions.

We next investigated the mechanical properties of P-cadherin during the adhesion using atomic force microscopy-based single-cell spectroscopy to measure the force of interaction between MeT5A cells cultured on plates and ovarian cancer cells attached to the cantilever (Figure 1D). HM cells exhibited a significantly higher rupture force compared to NM cells (Figure 1E), indicating the presence of stronger mechanical stress at the

(D) An image illustrating the measurement of cell-cell rupture forces by atomic force microscopy.

(E and F) Rupture forces of NM or HM detached from MeT5A cells (E), and HM detached from MeT5A cells in the absence or presence of siP-cad or P-cad blocking antibody (P-cad Ab), with siNS and IgG as controls, respectively (F) (n = 5).

(G) P-cad expression in normal ovarian surface epithelial (OSE) cells and ascites from patients with ovarian cancer (n = 7) were analyzed by western blot.

(H) Binding of Fc- or P-cad/Fc-coated beads to HM cells were quantified. Scale bar, 20 μm.

(I) Cell viability of HM cells treated with Fc- or P-cad/Fc-coated beads for 3 days were determined. All experiments were repeated three times. β-actin serves as the loading control. Data are presented as mean ± SD. *p < 0.05, **p < 0.01. See also Figure S1.

junctions between HM and MeT5A cells in contrast to the junctions between NM and MeT5A cells. The rupture force in HM-MeT5A interactions decreased when treated with siP-cad or a P-cadherin neutralizing antibody, compared to interactions treated with siNS or control immunoglobulin (Ig)G treatment, respectively (Figure 1F). These findings suggest that P-cadherin plays an essential role in mediating mechano-interactions between these two cell types. Notably, we also observed enhanced P-cadherin expression in ascitic tumor cells derived from patients with ovarian cancer compared to normal ovarian surface epithelium (OSE) (Figure 1G). Slight variations in the P-cadherin protein size were observed among different patients, likely due to differences in glycosylation.[23] To test the functional role of P-cadherin, we further used magnetic beads coated with immobilized P-cadherin Fc chimera protein (P-cad/Fc), which bind to the cell surface and mimic cadherin-mediated adhesion (Figure 1H).[24] The presence of P-cad/Fc-coated beads significantly enhanced cell proliferation in HM cells, whereas IgG Fc-coated beads showed no effect when compared with the untreated control (Figure 1I). These findings suggest a potential role of P-cadherin in promoting tumor growth.

P-cadherin rewires lipid metabolism in tumor cells

Metabolic reprogramming enables cancer cells to meet the increased demand for energy and biosynthetic precursors necessary for their uncontrolled growth during metastasis. The observed enhancement in proliferation resulting from P-cadherin-coated beads prompted us to hypothesize that P-cadherin affects cellular metabolism. To test this, we performed RNA sequencing (RNA-seq) of HM cells upon treatment with siNS or siP-cad. Pathway analysis revealed a significant alteration in fatty acid (FA) metabolism ($p < 0.05$; Figure 2A). To validate our RNA-seq findings, we performed RT-PCR for several key lipogenic genes, namely acetyl-coenzyme A (CoA) acetyltransferase 2 (ACAT2), ATP-citrate lyase (ACLY), FA synthase (FASN), lipin 1 (LPIN1), and sterol regulatory element-binding transcription factor 1 (SREBF1). All these genes exhibited significantly decreased expression in HM cells treated with siP-cad (Figure 2B). Consistently, overexpression of P-cadherin in NM cells led to the upregulated expression of these lipogenic genes (Figure 2B). Western blot further confirmed similar changes at the protein level (Figure S2A). We also tested the expression of well-known lipolytic genes, including hormone-sensitive lipase (HSL), monoacylglycerol lipase (MAGL), and perilipin-1 (PLIN), which remained unchanged regardless of P-cadherin expression (Figures 2B and S2A), confirming that P-cadherin specifically regulates lipogenesis rather than lipolysis in HM cells. Moreover, HM cells sorted from the MeT5A coculture showed significant upregulation of the above key lipogenic proteins compared to HM cells cultured alone (Figures 2C and S2B). This was supported by oil red O (ORO) staining, which revealed greater accumulation of neutral lipids in the HM-MeT5A coculture than in HM cells alone, whereas no change was observed in NM cells upon coculture (Figures 2D and S2C). Compared with IgG and siNS controls, P-cadherin antibody and siP-cad markedly impaired the lipid accumulation in HM cells, as revealed by decreased ORO staining in the HM-MeT5A coculture (Figures 2E and S2D).

Consistently, overexpression of P-cadherin in NM enhanced lipid accumulation upon coculture (Figure 2F). These observations collectively suggest a specific role of P-cadherin in regulating de novo lipogenesis in HM cells during mesothelial adhesion. We also pretreated HM cells with 5-(tetradecyloxy)-2-furoic acid (TOFA), which inhibits acetyl-CoA carboxylase essential for FA synthesis[24] or silenced SREBP1, which is a master regulator of lipogenesis.[25] Both treatments resulted in a significant decrease in cellular lipid content during the HM-MeT5A coculture (Figures 2G and 2H), suggesting that additional lipids are produced through de novo lipogenesis instead of being transferred from the extracellular environment.

We also performed Seahorse XF analysis to assess the influence of P-cadherin on bioenergetic metabolism in HM cells. Our results showed that siP-cad did not alter mitochondrial or glycolytic metabolism in HM cells (Figure 2I). Consistently, RT-PCR showed that siP-cad had no effect on the uptake of glucose or the expression of glycolytic genes, including glucose transporter 1 (GLUT1), hexokinase 2 (HK2), glucose-6-phosphate isomerase (GPI), and phosphoglycerate kinase 1 (PGK1), in HM cells (Figures S2E and S2F). Gene set enrichment analysis (GSEA) of RNA-seq data also suggested that the lipolytic or glycolytic pathways were unaffected (Figure S2G). Together, these results further indicate that P-cadherin-mediated tumor-mesothelium adhesion specifically evokes de novo lipogenesis in HM cells.

P-cadherin-mediated mechanotransduction regulates lipogenesis through SREBP1 activation

We next investigated the mechanistic basis for the link between P-cadherin-mediated mechanotransduction and cell metabolism. Among the lipogenic genes upregulated by P-cadherin, we chose to focus on SREBP1 (encoded by the SREBF1 gene) since it is an important transcription factor that regulates FA synthesis and has been shown to be mechanically regulated by extracellular matrix stiffness.[26,27] Treatment with P-cad/Fc beads led to the upregulation of SREBP1 mRNA as well as both the full-length (fl) precursor and mature (ma) forms of SREBP1 proteins in HM cells (Figure 3A). Immunostaining showed enhanced nuclear levels of SREBP1 upon P-cad/Fc bead treatment, an effect that could be inhibited by the P-cadherin blocking antibody (Figure 3B), confirming the specific role of P-cadherin in SREBP1 activation. The expression of lipogenic genes induced by P-cad/Fc-coated beads was found to be suppressed upon knockdown of SREBP1 (Figure 3C). Furthermore, the reduction in lipogenic gene expression caused by siP-cad could be restored by overexpressing SREBP1 (Figure 3D), further validating the involvement of SREBP1 in P-cadherin-mediated lipogenesis. To investigate how P-cadherin transduces this signal, we evaluated the effects of mechanical cues on the actin cytoskeleton. Phalloidin staining showed that P-cadherin-mediated adhesion force significantly enhanced filamentous actin tension, which was blocked by treatment with P-cadherin antibody (Figures 3E and 3F). Treatment of HM cells with blebbistatin, an inhibitor of myosin that disrupts actin organization, inhibited the induction of SREBP1 by P-cad/Fc-coated beads (Figure 3G). A reduction of cytoplasmic p120 catenin (p120ctn), along with active Rac1 and Cdc42—key mediators of cadherin-induced
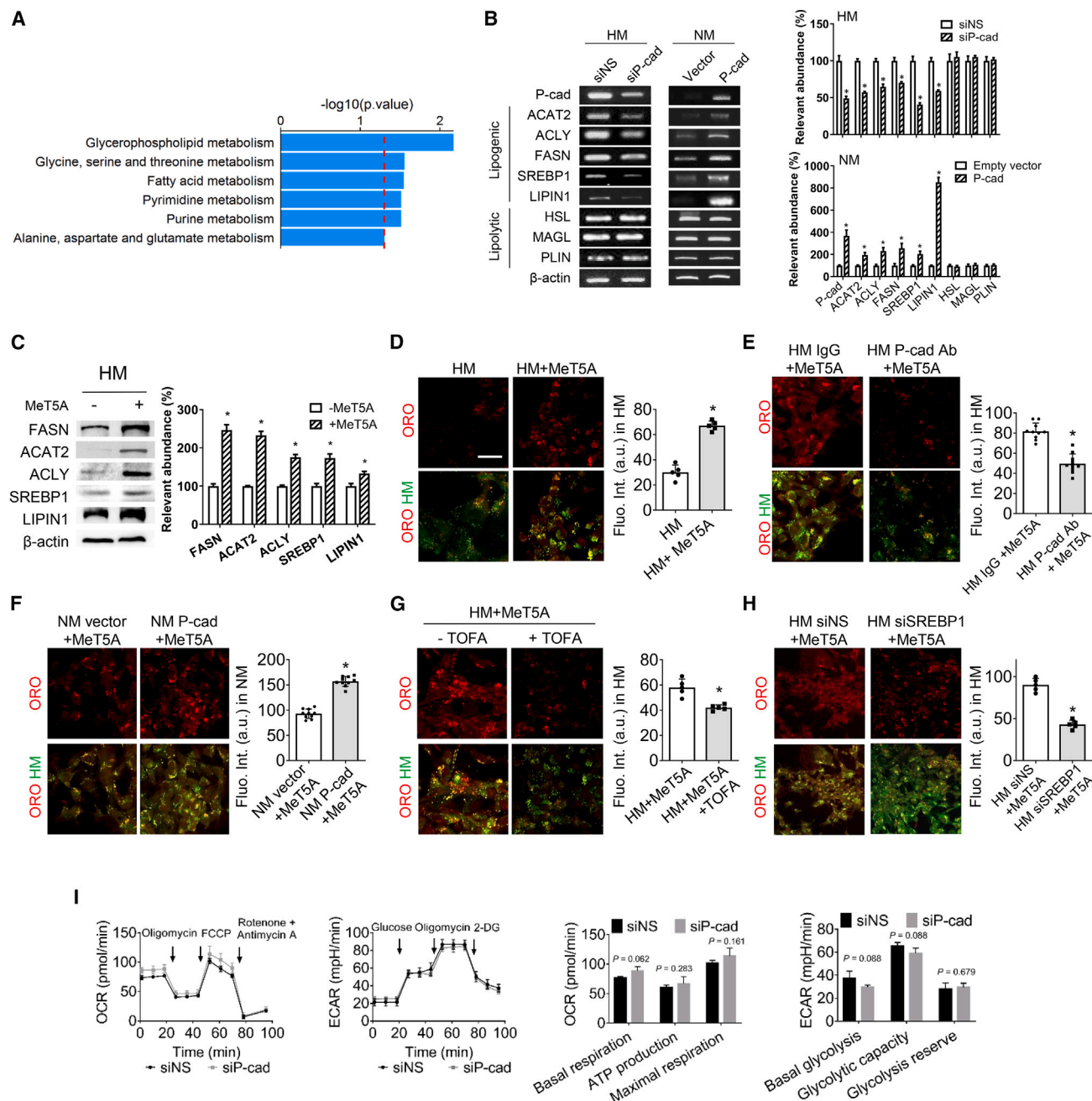
Figure 2. P-cadherin rewires lipid metabolism in tumor cells

(A) RNA-seq of siNS or siP-cad-treated HM cells identified pathways downregulated in siP-cad compared to siNS. Red line indicates $p = 0.05$.

(B) RT-PCR of P-cad, lipogenic genes (ACAT2, ACLY, FASN, SREBP1, and LIPIN1) and lipolytic genes (HSL, MAGL, and PLIN) in HM cells transfected with siNS, siP-cad, empty vector, or P-cad overexpression vector ($n = 3$).

(C) Western blot of FASN, ACAT2, ACLY, SREBP1, and LIPIN1 in HM cells cultured alone or cocultured with MeT5A ($n = 3$).

(D–H) Representative images and quantification of oil red O (ORO) staining of neutral lipids (red) in CMFDA-labeled HM or NM cells (green) cocultured with MeT5A are shown. (D) HM cells were cultured alone or cocultured with MeT5A. (E) HM cells were treated with P-cadherin antibody (P-cad Ab) or IgG isotype control before MeT5A coculture. (F) NM cells were transfected with P-cad overexpression vector or empty vector control before MeT5A coculture. (G) HM cells were pretreated with or without TOFA before MeT5A coculture. (H) HM cells were transfected with siNS or SREBP1 siRNA (siSREBP1) before MeT5A coculture.

(I) Mitochondrial metabolism (left) and glycolysis profiles (right) of HM cells treated with siNS or siP-cad and corresponding quantification of bioenergetic masses ($n = 4$ per group). β-actin serves as loading control. Scale bar, 20 μm. TOFA, 5-(tetradecyloxy)-2-furoic acid; OCR, oxygen consumption rate; ECAR, extracellular acidic rate. Data are presented as mean ± SD. *$p < 0.05$. Unpaired Student's t test for comparison between two groups and one-way ANOVA followed by a Tukey's test for comparison between three or more groups. See also Figure S2.
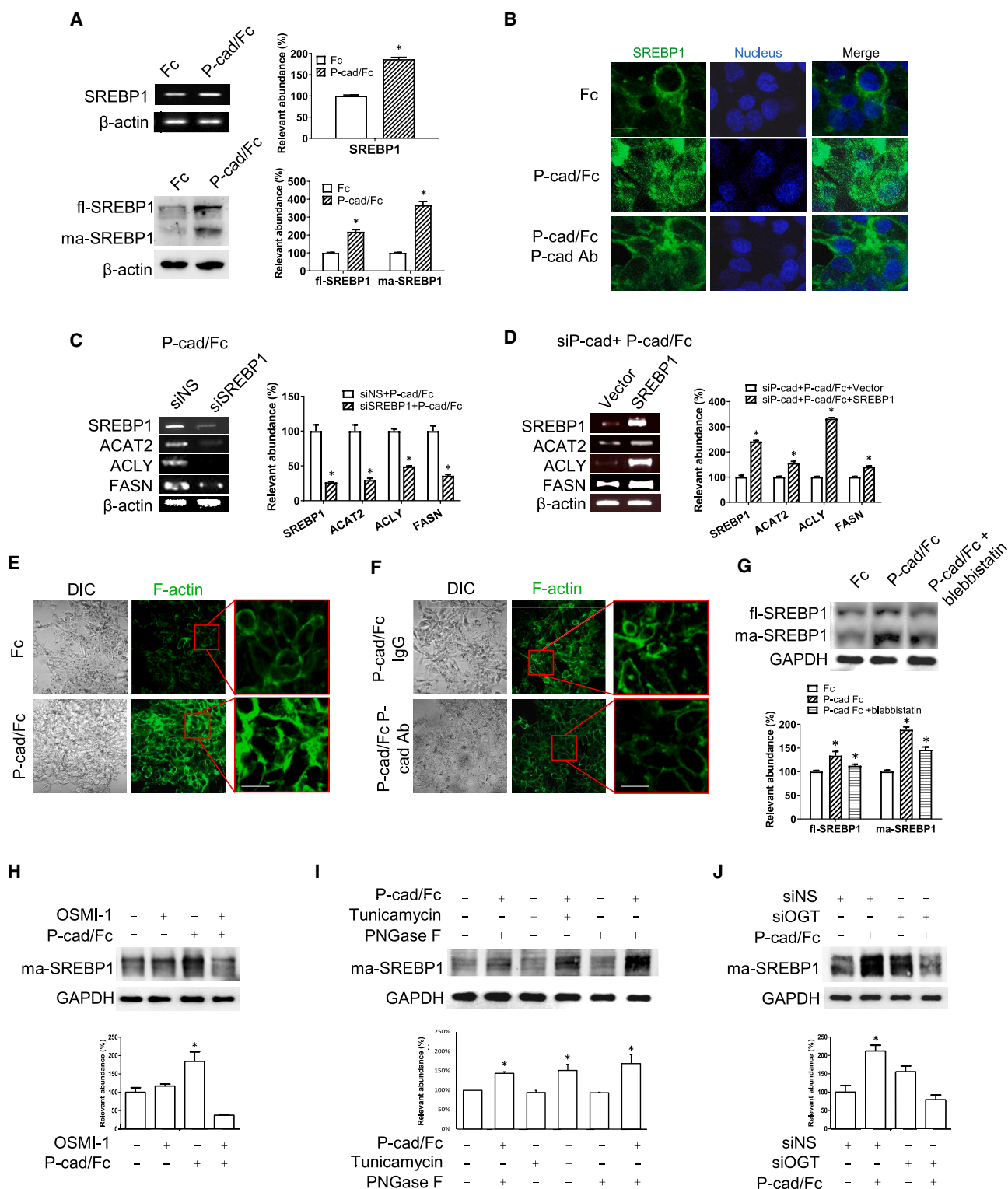
Figure 3. P-cadherin mechano-activates SREBP1 via actin remodeling in an O-GlcNacylation-dependent manner

(A) HM cells were treated with IgG/Fc (Fc)- or P-cad/Fc-coated beads followed by RT-PCR or western blot of SREBP1.

(B) Immunostaining of SREBP1 in HM cells after incubating with Fc- or P-cad/Fc-coated beads, with or without P-cadherin blocking antibody (P-cad Ab). Scale bar, 10 μm.

(C) RT-PCR of SREBP1, ACAT2, ACLY, and FASN in HM cells transfected with siNS or siSREBP1 in the presence of P-cad/Fc-coated beads.

(legend continued on next page)

actin remodeling[28]—was observed in HM cells treated with siP-cad and cocultured with MeT5A, further supporting P-cadherin-induced mechano-signal transduction in HM cells (Figures S2H and S2I).

Cell adhesion is controlled by dynamic posttranslational modifications (PTMs) that facilitate rapid biological responses to stimuli. O-GlcNAcylation, a widespread PTM that acts as an important sensor of metabolic state, has recently been linked to lipogenesis and the regulation of SREBP1.[29–31] O-GlcNAcylation of specificity protein 1 (Sp1) has been shown to enhance its binding to the SREBP1 promoter and activate transcription while also potentially increasing SREBP1 protein stability through its interaction with the E3-ubiquitin ligase FBW7.[29,31] Therefore, we asked if this PTM is involved in P-cadherin regulation on SREBP1. Treating HM cells with OSMI-1, an inhibitor of O-GlcNAc transferase (OGT), suppressed SREBP1 induction by P-cad/Fc-coated beads (Figure 3H). However, both treatment with tunicamycin, an inhibitor of N-glycan biosynthesis, and surface N-glycan removal by PNGase F had no effect on the induction of SREBP1 by P-cad/Fc-coated beads (Figure 3I). Consistent with OSMI-1 treatment, knockdown of OGT by an siRNA inhibited SREBP1 induction (Figure 3J). To demonstrate that O-GlcNAcylation regulates downstream lipogenesis by acting on SREBP1, we used the O-GlcNAcase inhibitor thiamet G, which enhances O-GlcNAcylation. Treatment with thiamet G increased the expression of lipogenic genes, an effect that was abolished by siSREBP1 (Figure S2J). These data together suggest that P-cadherin regulates SREBP1 in an O-GlcNAcylation-dependent manner.

P-cadherin activates glycolysis in mesothelial cells

We next determined whether tumor-mesothelial interaction could induce changes in the activity of mesothelial cells. Compared with MeT5A alone, HM, but not NM, cells selectively activated MeT5A to secrete tumor-promoting cytokines, such as granulocyte colony-stimulating factor (G-CSF), granulocyte-macrophage colony-stimulating factor (GM-CSF), IL-6, IL-8, CXCL1/GROα, and IL-1α/IL-1F1 (Figure 4A). As shown in Figure 4B, we noted a marked decrease in E-cadherin expression and a strong induction of N-cadherin and fibronectin expression in MeT5A sorted from the HM coculture compared with MeT5A alone. Similar results were observed using HPMC (Figure S3A), suggesting the presence of mesothelial-to-mesenchymal transition, which is indicative of mesothelial cell activation.[6]

Considering the impact of P-cadherin on HM metabolism, it is plausible that P-cadherin might also influence the metabolic profile of mesothelial cells. However, upon silencing P-cadherin, we observed no effect on the expression levels of lipogenic genes (Figures 4C and S3B). Interestingly, we discovered that treatment with siP-cad or P-cadherin overexpression led to a significant decrease or increase, respectively, in key glycolytic genes (GLUT1, HK2, GPI, and PGK1) in mesothelial cells (Figures 4D, S3C, and S3D). Corresponding changes at the protein level were observed by western blot (Figures S3B–S3D). Additionally, flow cytometric analysis revealed a reduced capacity of MeT5A cells to uptake glucose, as shown by a decrease in the fluorescence signal of 2-NBDG (a glucose analog) following siP-cad transfection compared to siNS transfection (Figure 4E). In contrast, treatment of MeT5A cells with P-cad/Fc-coated beads led to a significant increase in glucose uptake and subsequent lactate production, which was reversed by siP-cad treatment (Figures 4F and 4G). These findings provide compelling evidence that P-cadherin-mediated adhesion forces promote a highly glycolytic profile in mesothelial cells.

Lactate is shuttled to HM cells as a lipid source

Given the differential metabolic alterations mediated by P-cadherin in tumor and mesothelial cells, we postulated that the lactate produced by the activated mesothelium may drive HM tumor cell lipogenesis. We first traced the lipidomic fate of ^{13}C-labeled lactate in metastatic tumors in mice through gas chromatography-tandem mass spectrometry (GC-MS/MS) and found that palmitic acid (C16:0) in HM tumor cells was labeled to a larger degree (M + 2 to M + 8) than that in NM tumor cells (M + 2 to M + 4), indicating that HM cells use more lactate for de novo FA synthesis compared to NM cells (Figure S4A). To provide direct evidence that mesothelial cell-derived lactate could promote HM lipogenesis, we performed targeted lipidomics in the HM-MeT5A coculture after incubation with uniformly ^{13}C-labeled glucose ([U^{13}C$_6$]-glucose) with or without the addition of cold lactate (Figure 5A). In the presence of cold lactate, the generation of high ^{13}C-labeled palmitic acids was shifted to low ^{13}C-labeled palmitic acid (16:0) in the sorted HM cells (Figure 5B). Similar results were observed for palmitoleic acid (16:1) and cholesterol synthesis (Figure 5B), confirming that MeT5A-secreted lactate is used by HM cells for lipid generation (Figure 5C). Consistently, siP-cad reduced the lactate uptake of HM induced by P-cad/Fc-coated beads (Figure S4B).

We also performed ^{13}C glucose experiment to confirm the role of P-cadherin in lactate shuttling during coculture. Comparing to siNS control, siP-cad caused a significant decrease in ^{13}C-labeled palmitic acid (M + 14) and palmitoleic acid (M + 12 to M + 16) in HM cells, suggesting a role of P-cadherin in lipogenesis (Figure 5D). There was also a significant reduction in ^{13}C-labeled pyruvate, while no difference was found in phosphoenolpyruvate, a metabolic product upstream of pyruvate in the glycolytic pathway (Figure 5D). These data support our results

---

(D) HM cells were co-transfected with siP-cad and empty vector or SREBP1 overexpression vector, followed by incubation with P-cad/Fc-coated beads. RT-PCR of the indicated genes was performed.

(E and F) Phalloidin staining of F-actin in HM cells treated with Fc- or P-cad/Fc-coated beads (E) and in HM cells treated with or without P-cad antibody in the presence of P-cad/Fc-coated beads (F). Scale bar, 20 μm.

(G) Expression of full-length (fl)- and mature (ma)-SREBP1 in HM cells with the indicated treatment were analyzed by western blot.

(H) HM cells were treated with beads coated with Fc or P-cad/Fc and OSMI-1 as indicated, followed by western blot.

(I) HM were treated with tunicamycin, PNGase F and Fc- or P-cad/Fc-coated beads as indicated, followed by western blot.

(J) HM cells transfected with siNS or OGT siRNA (siOGT) were treated with Fc- or P-cad/Fc-coated beads, followed by western blot. β-actin and GAPDH serve as loading controls. Data are presented as mean ± SD from three independent experiments. *p < 0.05. Unpaired Student's t test for comparison between two groups and one-way ANOVA followed by a Tukey's test for comparison between three or more groups.
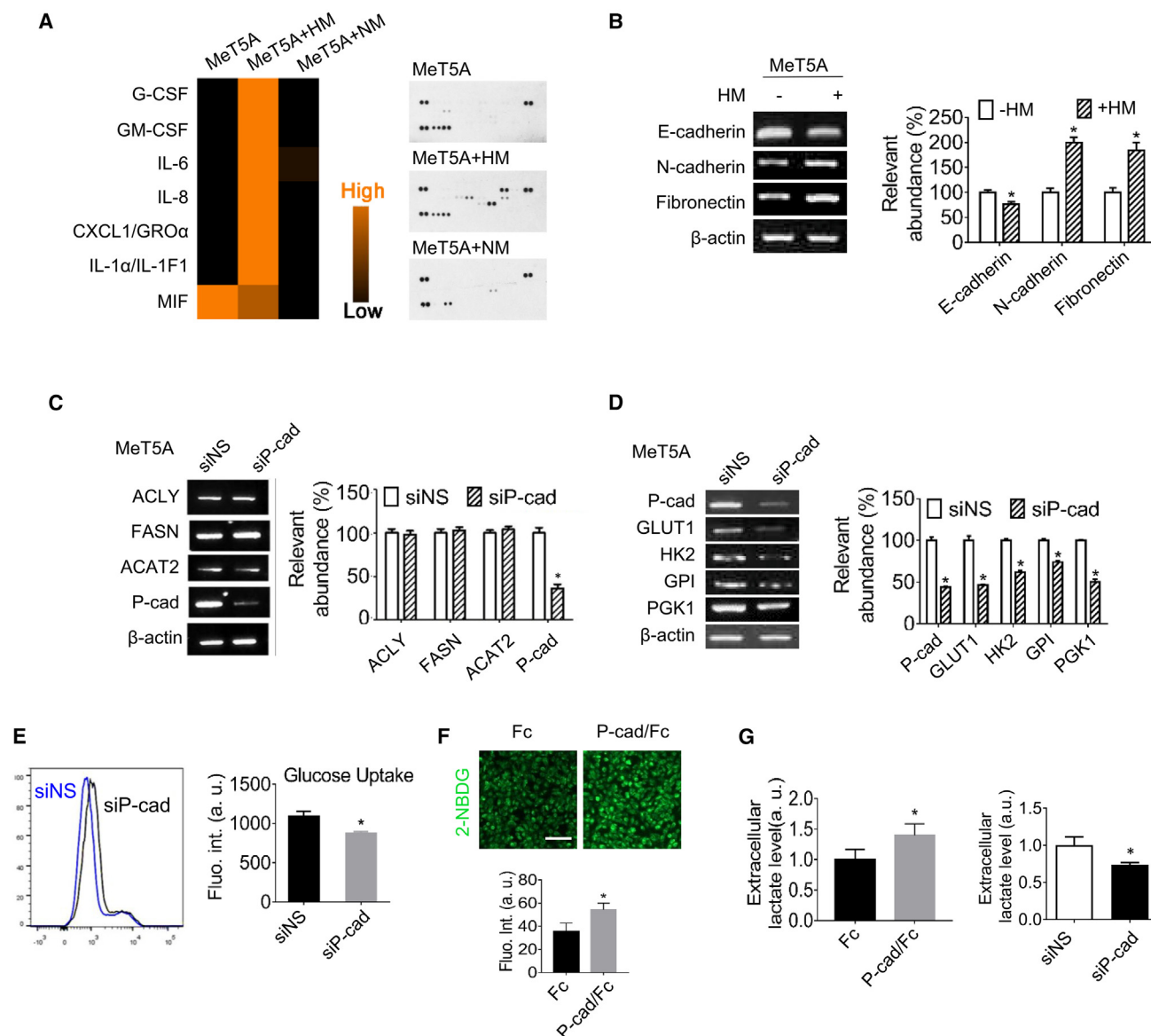
Figure 4. P-cadherin regulates glycolysis in MeT5A cells
(A) Cytokine array analysis of conditioned medium from MeT5A alone or cocultured with HM or NM cells.
(B) RT-PCR analysis of E-cadherin, N-cadherin, and fibronectin levels in MeT5A cocultured with or without HM.
(C and D) MeT5A cells transfected with siNS or siP-cad were cocultured with HM. After coculture, flow-sorted MeT5A cells were analyzed by RT-PCR for (C) P-cad and lipogenic genes (ACAT2, ACLY, and FASN) and (D) P-cad and glycolytic genes (GLUT1, HK2, GPI, and PGK1). β-actin serves as the loading control.
(E) Glucose uptake in siNS or siP-cad-treated MeT5A cells was analyzed by flow cytometry using the glucose analog 2-[N-(7-nitrobenz-2-oxa-1,3-diazol-4-yl)amino]-2-deoxy-D-glucose (2-NBDG).
(F) Representative fluorescent images of 2-NBDG uptake by MeT5A treated with Fc- or P-cad/Fc-coated beads for 24 h, and quantification of fluorescent intensity ($n = 10$), are shown.
(G) Extracellular lactate levels in the conditioned medium of MeT5A cells treated with Fc- or P-cad/Fc-coated beads (left) and siNS or siP-cad (right) were measured. Data are presented as mean ± SD from three independent experiments. *$p < 0.05$. Unpaired Student's t test for comparison between two groups and one-way ANOVA followed by a Tukey's test for comparison between three or more groups. See also Figure S3.

that P-cadherin did not affect the glycolysis pathway but may affect the use of ^{13}C-labeled lactate from MeT5A as a source for lipogenesis.

We hypothesized that lactate shuttling is important for tumor-mesothelial interaction. Monocarboxylate transporter 4 (MCT4) and monocarboxylate transporter 1 (MCT1) are the major transporters of lactate efflux and uptake, respectively.[32,33] As shown in Figures 5E and 5F, suppressing lactate export in MeT5A with siMCT4 restricted both HM cell proliferation and lipid generation during coculture. Alternatively, inhibiting lactate import by MCT1
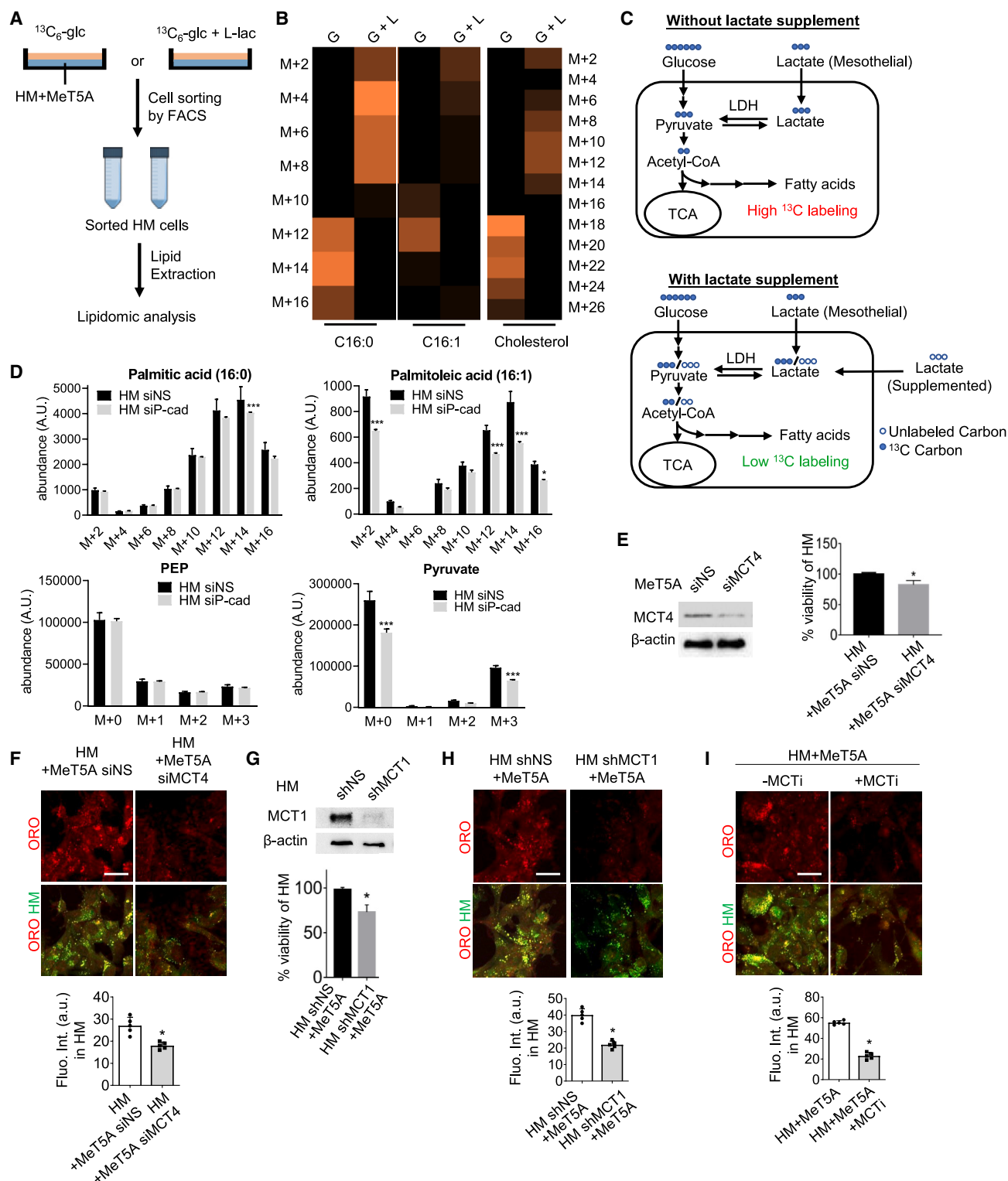
Figure 5. Lactate is shuttled from mesothelial cells into HM cells

(A) Schematic illustration of the ^{13}C-labeled targeted lipidomic assay workflow.

(B) Heatmap of ^{13}C-labeled fatty acids and cholesterol (C16:0, C16:1, CHOL) in sorted HM cells.

(C) Schematic illustration of the expected effects of supplemented cold lactate on lipid composition.

(legend continued on next page)

short hairpin RNA (shRNA) in HM cells abolished proliferation and lipid accumulation (Figures 5G and 5H). AR-C155858,[34] a MCT1/2 inhibitor, was also used to block lactate uptake in HM cells. AR-C155858 significantly reduced the ORO staining in the HM-MeT5A coculture, further confirming that lactate shuttling is required for lipogenesis in tumor cells (Figure 5I). These results demonstrate that P-cadherin-mediated adhesion drives *de novo* lipogenesis in highly metastatic tumor cells through the vectorial transport of lactate from the mesothelium to cancer cells.

High FASN expression is associated with high P-cadherin and Ki67 expression in patients with metastatic ovarian cancer

To corroborate the clinical relevance of lipogenesis in peritoneal metastasis, we first performed immunohistochemical staining of FASN in paired primary and metastatic tumor samples obtained from patients with high-grade serous ovarian carcinoma. The metastatic samples include omental metastases as well as metastatic specimens from other sites with mesothelial lining (total $n = 16$: omentum, $n = 9$; bladder flap, $n = 4$; pelvic peritoneum/peritoneal, $n = 3$). The clinicopathological information is provided in Table S1. We specifically examined the FASN expression in tumor cells rather than adipocytes, which are histologically distinct. As shown in Figures 6A and 6B, the majority of metastatic specimens expressed elevated levels of tumor FASN (H-score) as compared to their parallel primary samples (10 of 16 metastatic specimens, 62.5%, $p = 0.0362$). To validate the association between FASN, P-cadherin, and metastatic growth, we further evaluated the expression levels of P-cadherin and the proliferation marker Ki67. Metastatic specimens with elevated FASN expression showed higher expression of P-cadherin and Ki67 compared to matched primary tumors (P-cadherin, $p = 0.0340$; Ki67, $p = 0.0241$), while metastatic specimens with low FASN expression showed little change in P-cadherin and Ki67 expression (Figures 6C and 6D). The higher expression levels of FASN, P-cadherin, and Ki67 in HM relative to NM tumors were also confirmed (Figures S5A and S5B). These data support the association of P-cadherin with cell proliferation through lipogenic regulation.

To confirm the importance of P-cadherin signaling *in vivo*, we used our well-characterized amphiphilic dendrimers, AmDM, which formed nanoparticles with siRNA and could specifically target tumor sites through enhanced permeation and retention effect.[35,36] Mice with intraperitoneal xenograft of HM were treated with dendriplexes of siP-cad, which caused significant reductions in the number of metastatic tumor nodules and ascites formation in the peritoneal cavity, as well as enhanced sur-

vival as compared with mice injected with control dendriplexes of siNS (Figures 6E and 6F). A representative high-magnification image of the tumor nodules and histological H&E staining are shown in Figures S6A and S6B to confirm the identification of metastatic tumors. Successful P-cadherin knockdown using dendriplexes was confirmed by western blot (Figure S6C). Additionally, siP-cad dendriplexes *in vivo* significantly reduced the expression lipogenic genes ACLY, FASN, ACAT2, and lactate transporter MCT4 of the metastatic tumors (Figure S6D). These data validated an important role of P-cadherin in metabolic reprogramming during metastasis.

Inhibition of MCT1/4 reduces peritoneal metastasis *in vivo*

High expression of MCT1 was found to be significantly associated with a decrease in both overall survival and progression-free survival of patients with ovarian cancer using Kaplan-Meier plotter ($p < 0.005$) (Figure 7A). MCT1 also showed a positive correlation with P-cadherin and FASN expression (Figure 7B), implicating the importance of the lactate uptake. To further confirm lactate shuttling *in vivo*, mice bearing intraperitoneal HM tumors were treated with dendriplexes of siMCT1 or siMCT4. Successful target gene knockdown using dendriplexes was confirmed by western blot (Figure S6C). We observed significant reductions in the number of metastatic tumor nodules and ascites formation compared to mice injected with siNS-dendriplexes control (Figures 7C and 7E). Kaplan-Meier curves showed that mice with specific targeting of MCT1 or MCT4 also displayed prolonged survival (Figures 7D and 7F). The importance of MCT1 in peritoneal metastasis was also supported by shRNA knockdown (Figure S6E). We further demonstrated the potential of therapeutic targeting by treatment with a clinical-grade MCT1 inhibitor, AZD3965,[37] which significantly reduced metastasis in mice (Figure S6F). These *in vivo* experiments, together with patient analysis, strongly support the clinical importance of our proposed mechanisms in ovarian cancer metastasis.

DISCUSSION

Adhesion to the mesothelium and the ability to sustain proliferation at the secondary site are pivotal events in peritoneal metastasis; however, the underlying mechanisms remain poorly elucidated. In this study, we have identified P-cadherin as a distinct and critical mediator that initiates metabolic symbiosis between tumor cells and the interacting mesothelium. These findings are consistent with preclinical and clinical evidence, which suggest a correlation between high expression of P-cadherin, metastasis, and unfavorable clinical outcomes in ovarian cancer,[38–41] thereby

(D) Lipidomic analysis of ^{13}C-labeled palmitic acid (C16:0), palmitoleic acid (C16:1), and glycolysis intermediates phosphoenolpyruvate (PEP) and pyruvate in HM cells with siNS or siP-cad after coculture with MeT5A in medium supplemented with 25 mM [U^{13}C]-glucose (with three technical replicates each). Data are presented as mean ± SD. *$p < 0.05$, ***$p < 0.001$. Two-way ANOVA.

(E and F) HM cells were cocultured with MeT5A transfected with non-specific or MCT4 siRNA (siNS or siMCT4). MCT4 expression in MeT5A cells was analyzed by western blot, and HM cell viability was assessed (E). Representative images and quantification of ORO staining in CMFDA-labeled HM (green) are shown (F).

(G and H) HM with non-specific or MCT1 shRNA (shNS or shMCT1) were cocultured with MeT5A. MCT1 expression in HM cells was analyzed by western blot, and HM cell viability was assessed (G). Representative images and quantification of ORO staining (red) in HM (green) are shown (H).

(I) Representative images and quantification of ORO staining (red) in HM (green) in the absence or presence of monocarboxylate transporter inhibitor (MCTi) and MeT5A coculture are shown. Scale bar, 20 μm. β-actin was used as the loading control for all western blots ($n = 3$). Data are presented as mean ± SD. *$p < 0.05$. Unpaired Student's t test. See also Figure S4.
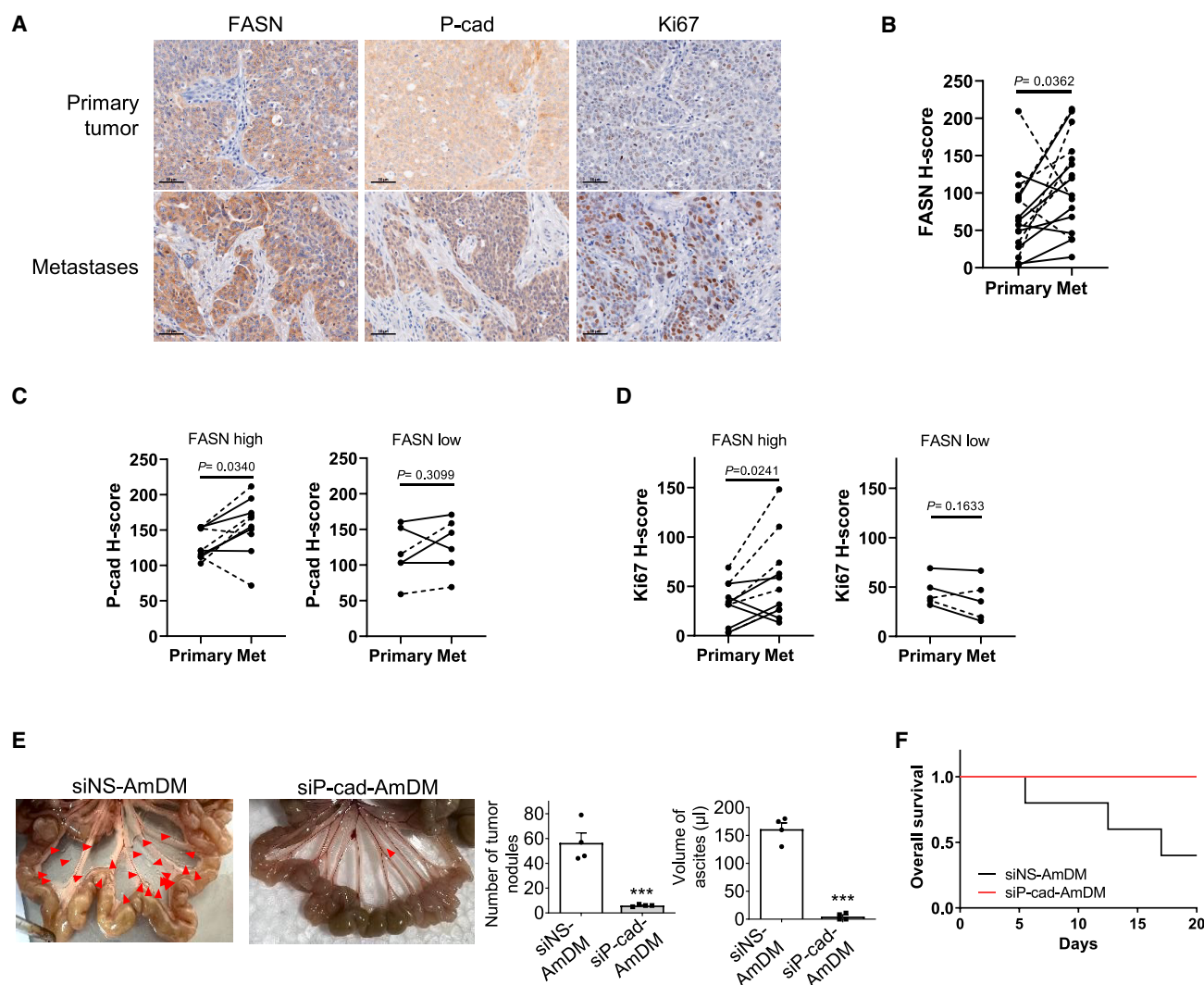
Figure 6. High FASN expression is associated with high P-cadherin and Ki67 expression in metastatic ovarian cancer

Immunohistochemistry (IHC) analysis of FASN, P-cad, and the proliferation marker Ki67 expression was performed in primary patient specimens ($n = 10$) and paired metastatic specimens of omental and other peritoneal sites ($n = 16$).

(A) Representative images of IHC staining of FASN, P-cad, and Ki67 are shown. Scale bar, 50 μm.

(B) Quantitative analysis (H-score) of FASN expression in paired primary and metastatic specimens of omental (solid lines) and other peritoneal sites (dashed lines).

(C and D) Quantitative analysis of P-cad (C) or Ki67 (D) expression in patients with elevated metastatic FASN expression vs. low metastatic FASN expression. Data presented are median value. Paired Student's t test; $p < 0.05$ is considered significant.

(E and F) Mice were intraperitoneally injected with HM cells followed by intravenous injection of siNS-AmDM or siP-cad-AmDM for 3 weeks. Representative images of the peritoneal metastases and quantification of tumor nodules and ascites volume are shown ($n = 5$) (E). Data are presented as mean ± SD. Unpaired Student's t test, ***$p < 0.001$. (F) Kaplan-Meier curves show survival of mice with siNS-AmDM and siP-cad-AmDM treatment. See also Figure S5 and Table S1.

emphasizing the therapeutic potential of targeting P-cadherin in the management of peritoneal metastasis. Although the current study did not investigate the mechanism by which P-cadherin is upregulated in metastatic cells, our previous research and unpublished data suggest that P-cadherin may be upregulated transcriptionally or post-translationally by gonadotropin-releasing hormone (GnRH) or hepatocyte growth factor (HGF).[28] While cadherin-mediated adhesion typically occurs within a complex milieu where diverse cell types engage in physical interac-

tions, the majority of cadherin studies have predominantly focused on homotypic interactions among cells of the same lineage. In contrast, our results clearly show that homophilic interactions mediated by P-cadherin could elicit distinct signaling responses in tumor and mesothelial cells at the secondary site. This finding provides invaluable insights into the spatial dynamics of cadherin adhesion and signaling during the metastatic process. Moreover, this specific metabolic coupling may underlie the organotropism of metastatic cells toward the peritoneum,
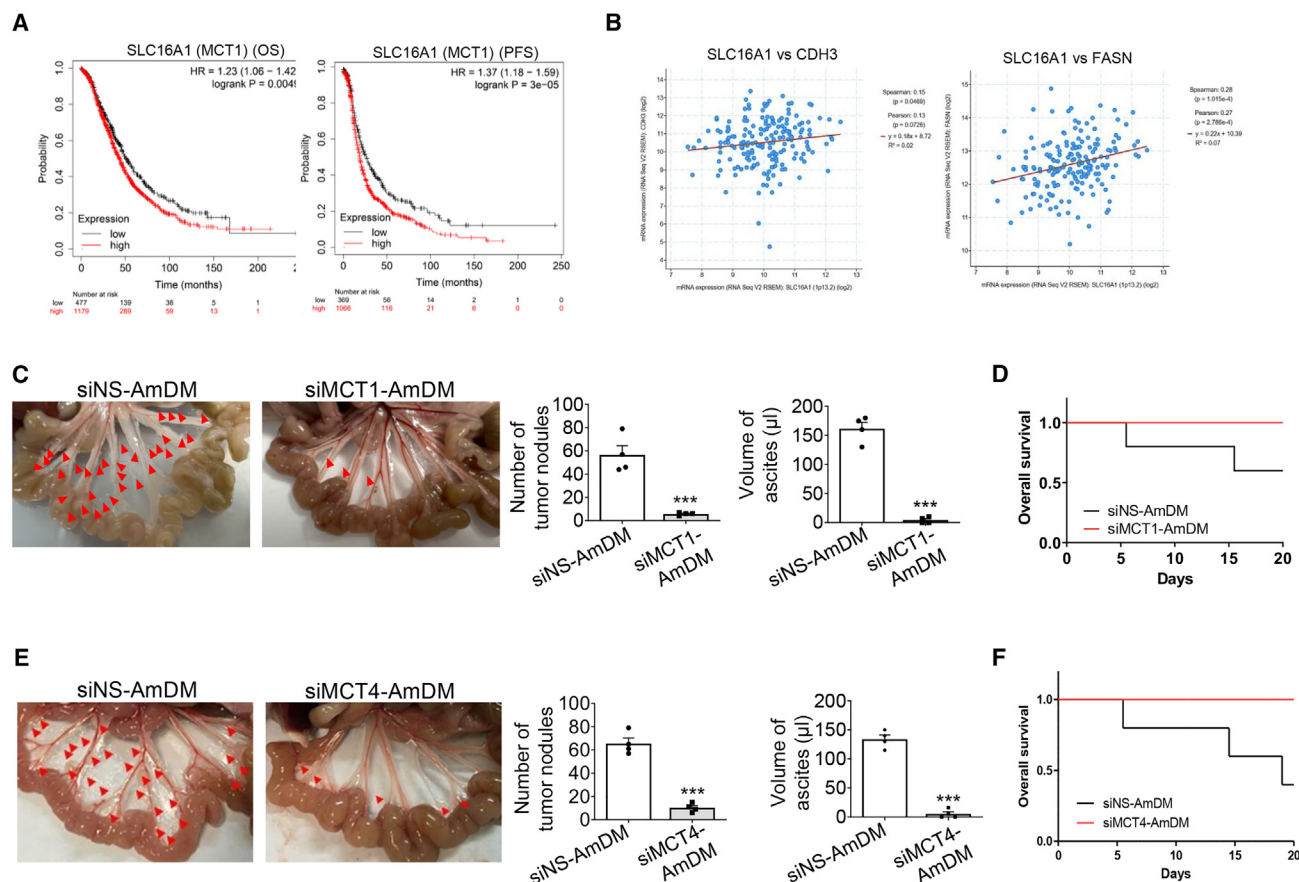
Figure 7. MCT1/MCT4-mediated lactate shuttling is a potential therapeutic target for peritoneal metastasis

(A) Kaplan-Meier plot of overall survival (OS) and progression-free survival (PFS) in ovarian cancer patients with low and high expression of MCT1. Number at risk is listed below.

(B) SLC16A1 (MCT1) mRNA transcript level positively correlates with CDH3 (P-cad) and FASN transcript levels.

(C–F) Mice bearing intraperitoneally injected HM cells were intravenously injected with siNS-AmDM or siMCT1-AmDM (C and D) and siNS-AmDM or siMCT4-AmDM (E and F) for 3 weeks. Representative images of the peritoneal metastases and quantification of tumor nodules and ascites volume are shown ($n = 4$). (D and F) Kaplan-Meier curves show OS of mice with siNS-AmDM, siMCT1-AmDM, or siMCT4-AmDM treatment as indicated. Data are expressed as mean ± SEM. Unpaired Student's t test, ***$p < 0.001$. See also Figure S6.

potentially influencing the prognosis and treatment strategies for cancer patients.

How mechanical pathways are integrated with other cellular processes, such as cell metabolism, remains largely unknown. Our findings indicate that P-cadherin has distinct roles in regulating metabolic pathways in mesothelial versus metastatic tumor cells. P-cadherin was shown to promote anoikis resistance by activating the pentose-phosphate pathway and reducing oxidative stress.[42] In addition, P-cadherin was associated with a hypoxic and glycolytic phenotype characterized by the expression of HIF-1α, GLUT1, CAIX, MCT1, and CD147.[43] It is possible that, in mesothelial cells, P-cadherin binding enhances glycolytic activity through signaling cascades involving hypoxia-inducible factors (HIFs) or AMPK, which promote glycolysis under metabolic stress or low-oxygen conditions. The hyperglycolytic phenotype of the mesothelium has been reported to promote mesothelial-to-mesenchymal transition and peritoneal fibrogenesis,[44] potentially reinforcing the metastatic process.

In contrast to mesothelial cells, metastatic cells are characterized by high aggressiveness and rapid proliferation and would require increased lipogenesis for energy storage. Previous research indicates that elevated extracellular matrix stiffness inhibits SREBP1 activity through increased acto-myosin contraction and AMPK activation.[26] The distinct signaling in HM cells could be attributed to the context-dependent mechanotransduction processes occurring at cell-matrix and cell-cell adhesion sites.[45] Moreover, the interaction between P-cadherin with other signaling molecules, such as insulin-like growth factor 1 receptor (IGF1R), may also contribute to the lipogenic processes in metastatic cells, as IGF1 signaling is often dysregulated in ovarian cancer and linked to increased lipogenic activity, which may involve SREBP1.[46–48] Notably, elevated SREBP1 expression has been correlated with advanced disease stages and poor prognosis in ovarian cancer and other malignancies.[25,49] Overall, the differential effects of P-cadherin on metabolic pathways reflect the unique signaling cascades and

metabolic needs of mesothelial and tumor cells, which could be shaped by the tumor microenvironment.

Lipids play a causal role in driving tumorigenesis and metastasis.[50] Overexpression of lipogenic genes has been associated with metastatic progression and poor prognosis in many cancer types. In ovarian cancer, the increased expression of FASN is observed in tumor tissues and predicts advanced disease status and poor clinical outcomes.[51] Inhibition of lipid metabolism using an inhibitor cocktail was shown to reduce the peritoneal metastasis of ovarian cancer *in vivo*.[52] Consistent with these findings, our data suggest that a P-cadherin-mediated lipogenic phenotype characterized by the overexpression of lipogenic genes is important for metastasis *in vivo*. Beyond serving as an energy source or building blocks for membrane synthesis, lipids play other important roles in the tumor microenvironment. For example, FAs and cholesterol enhance therapeutic resistance and impact immune cell functions.[53,54] The lipid pool in cancer cells can be supplied by both intracellular and extracellular sources, although the exact stoichiometric relationships between these sources remain to be determined.[55] Various cancers, including ovarian cancer, have been shown to uptake FAs produced by surrounding adipose tissues.[56] However, in some contexts such as autophagy in adipocytes and mitosis in cancer cells,[57,58] exogenously supplemented FAs could not fully compensate for *de novo*-synthesized FAs, suggesting that *de novo* lipogenesis is required for specific cellular processes. Furthermore, *de novo* lipogenesis may enable cancer cells to tailor their FA composition to meet their unique requirements. Notable differences in FA composition have been observed between omental fat deposits and malignant ovarian tumors. In addition, FA species vary in their length and saturation, and such diversity indicates that their availability depends on the specificity of metabolic pathways. Recent studies have shown that unsaturated FAs were enriched in ovarian cancer stem cells and were essential for their proliferation and survival.[59] Therefore, *de novo* lipogenesis may enable cancer cells to tightly control their FA composition. Moreover, metabolic intermediates in *de novo* lipogenesis (citrate, acetyl-CoA, malonyl-CoA, and palmitate) can function as secondary messengers for other signaling pathways.[60] Thus, the high lipid demand for metastatic growth is met not only by the tumor microenvironment but also by cancer cells themselves, making lipogenesis an attractive target for therapy.

Emerging evidence suggests lactate as an oncometabolite in the tumor microenvironment. For example, lactate was shown to promote the immunosuppressive function of regulatory T (Treg) cells through lactylation.[61] Significantly higher lactate levels were found in ovarian cancer peritoneal metastasis samples than in benign samples in a small cohort of patients.[62] Furthermore, high lactate transporter expression predicted advanced disease status and poor clinical outcomes in ovarian cancer.[63] Our study has demonstrated a proof of concept for the therapeutic targeting of P-cadherin, MCT1, or MCT4 using nanoparticle delivery. No mice exhibited apparent signs of toxicity, such as decreased food intake or activity or body weight loss, upon AmDM-siRNA treatment (data not shown). Dendrimer-based nanoparticles have received US Food and Drug Administration (FDA) approval and are currently being used in

clinical settings, with several ongoing clinical trials investigating their safety and efficacy for various diseases. Therefore, dendriplexes represent a promising therapeutic approach for targeting P-cadherin in patients. Alternatively, P-cadherin-specific antibodies could also be utilized. The peritoneal dissemination may offer a clinical advantage in that therapeutic genes may be sensitive and specific to target cells owing to the closed space of the peritoneal cavity.

In conclusion, this study has uncovered a mechanism by which metastatic cells utilize adhesion-driven mechanical cues to shape their metastatic niche and promote metastatic outgrowth. Our findings emphasize the crucial role of P-cadherin in connecting mechanotransduction and cell metabolism within the peritoneal metastatic niche. Targeting the unique mechanoresponsive metabolic vulnerabilities of cancer cells and the tumor microenvironment holds promise for precise and localized therapeutic interventions, reducing side effects and overcoming treatment resistance. These findings may extend beyond ovarian cancer, as P-cadherin is also upregulated in other cancer types like gastric, pancreatic, and colon cancers, where peritoneal metastasis represents a significant pathological process.

Limitations of the study

In this study, we aimed to investigate the role of specific cadherins in tumor cell-mesothelium adhesion; therefore, we only focused on those particularly relevant to ovarian cancer, namely P-cad, N-cad, E-cad, cad-17, and cad-6.[20,64–67] However, this targeted approach may introduce bias, as other adhesion molecules that could also contribute to intercellular adhesion and metabolic reprogramming were not included. Moreover, while our study demonstrates that mesothelial cells may be a significant source of lactate to promote tumor cell lipogenesis upon adhesion, we did not examine other cell types within the tumor microenvironment that could also contribute to lactate production.

RESOURCE AVAILABILITY

Lead contact
Requests for further information and resources should be directed to and will be fulfilled by the lead contact, Alice S.T. Wong (awong1@hku.hk).

Materials availability
This study did not generate new unique reagents.

Data and code availability
- RNA-seq data have been deposited in the Genome Sequence Archive (China National Center for Bioinformation) (GSA-Human: HRA004687) and are available upon request to J.M.
- This paper does not report original code.
- Any additional information required to reanalyze the data reported in this paper is available from the lead contact upon request.

AUTHOR CONTRIBUTIONS

J.M., S.K.Y.T., K.S.W.F., and K.W. conceived and performed the experiments, analyzed data, and prepared the manuscript. J.Z. performed the bioinformatics analysis. S.Y. and T.M.C. provided primary HPMCs. C.C.L.W. assisted with the lactate assay. P.P.C.I. provided clinical samples. L.P. provided dendrimers. C.B.C., A.H.W.N., and H.-Y.G. provided key knowledge. C.B.C. and A.S.T.W. supervised the study.

DECLARATION OF INTERESTS

The authors declare no conflict of interests.

STAR★METHODS

Detailed methods are provided in the online version of this paper and include the following:

- KEY RESOURCES TABLE
- EXPERIMENTAL MODEL AND STUDY PARTICIPANT DETAILS
  - Cell lines
  - Primary cell cultures and human patient samples
  - Mice
- METHOD DETAILS
  - Transfection and inhibitor treatment
  - Cell adhesion assay
  - Single-cell force spectroscopy
  - Western blot analysis
  - Detection of active Rac1, Cdc42
  - Fluorescence staining
  - Oil red O (ORO) staining
  - Glucose uptake assay
  - L-lactate measurement
  - Seahorse extracellular flux analysis
  - Proliferation assay
  - $^{13}C_6$-glucose and lactate competition assay
  - ^{13}C-metabolic flux analysis
  - Cell sorting
  - Treatment with Fc- or P-cadherin/Fc-coated beads
  - RNA extraction and reverse-transcription PCR analysis
  - RNA sequencing and data analysis
  - siRNA dendriplexes formation
  - Immunohistochemistry
  - Detection of active Rac1, Cdc42
- QUANTIFICATION AND STATISTICAL ANALYSIS

SUPPLEMENTAL INFORMATION

Supplemental information can be found online at https://doi.org/10.1016/j.celrep.2024.115096.

REFERENCES

1. Lengyel, E. (2010). Ovarian cancer development and metastasis. Am. J. Pathol. 177, 1053–1064. https://doi.org/10.2353/AJPATH.2010.100105.

2. Tan, D.S.P., Agarwal, R., and Kaye, S.B. (2006). Mechanisms of transcoelomic metastasis in ovarian cancer. Lancet Oncol. 7, 925–934. https://doi.org/10.1016/S1470-2045(06)70939-1.

3. Lheureux, S., Braunstein, M., and Oza, A.M. (2019). Epithelial ovarian cancer: Evolution of management in the era of precision medicine. CA Cancer J. Clin. 69, 280–304. https://doi.org/10.3322/CAAC.21559.

4. Chiang, A.C., and Massagué, J. (2008). Molecular basis of metastasis. N. Engl. J. Med. 359, 2814–2823. https://doi.org/10.1056/NEJMRA0805239.

5. de Visser, K.E., and Joyce, J.A. (2023). The evolving tumor microenvironment: From cancer initiation to metastatic outgrowth. Cancer Cell 41, 374–403. https://doi.org/10.1016/J.CCELL.2023.02.016.

6. Kenny, H.A., Chiang, C.Y., White, E.A., Schryver, E.M., Habis, M., Romero, I.L., Ladanyi, A., Penicka, C.V., George, J., Matlin, K., et al. (2014). Mesothelial cells promote early ovarian cancer metastasis through fibronectin secretion. J. Clin. Invest. 124, 4614–4628. https://doi.org/10.1172/JCI74778.

7. Natarajan, S., Foreman, K.M., Soriano, M.I., Rossen, N.S., Shehade, H., Fregoso, D.R., Eggold, J.T., Krishnan, V., Dorigo, O., Krieg, A.J., et al. (2019). Collagen remodeling in the hypoxic tumor-mesothelial niche promotes ovarian cancer metastasis. Cancer Res. 79, 2271–2284. https://doi.org/10.1158/0008-5472.CAN-18-2616.

8. Zheng, A., Wei, Y., Zhao, Y., Zhang, T., and Ma, X. (2022). The role of cancer-associated mesothelial cells in the progression and therapy of ovarian cancer. Front. Immunol. 13, 1013506. https://doi.org/10.3389/FIMMU.2022.1013506.

9. Bajwa, P., Kordylewicz, K., Bilecz, A., Lastra, R.R., Wroblewski, K., Rinkevich, Y., Lengyel, E., and Kenny, H.A. (2023). Cancer-associated mesothelial cell-derived ANGPTL4 and STC1 promote the early steps of ovarian cancer metastasis. JCI Insight 8, e163019. https://doi.org/10.1172/JCI.INSIGHT.163019.

10. Huang, H., Wang, Z., Zhang, Y., Pradhan, R.N., Ganguly, D., Chandra, R., Murimwa, G., Wright, S., Gu, X., Maddipati, R., et al. (2022). Mesothelial cell-derived antigen-presenting cancer-associated fibroblasts induce expansion of regulatory T cells in pancreatic cancer. Cancer Cell 40, 656–673.e7. https://doi.org/10.1016/J.CCELL.2022.04.011.

11. Qian, J., LeSavage, B.L., Hubka, K.M., Ma, C., Natarajan, S., Eggold, J.T., Xiao, Y., Fuh, K.C., Krishnan, V., Enejder, A., et al. (2021). Cancer-associated mesothelial cells promote ovarian cancer chemoresistance through paracrine osteopontin signaling. J. Clin. Invest. 131, e146186. https://doi.org/10.1172/JCI146186.

12. Jaalouk, D.E., and Lammerding, J. (2009). Mechanotransduction gone awry. Nat. Rev. Mol. Cell Biol. 10, 63–73. https://doi.org/10.1038/nrm2597.

13. Papavassiliou, K.A., Basdra, E.K., and Papavassiliou, A.G. (2023). The emerging promise of tumour mechanobiology in cancer treatment. Eur. J. Cancer 190, 112938. https://doi.org/10.1016/J.EJCA.2023.112938.

14. Hoffman, B.D., and Yap, A.S. (2015). Towards a dynamic understanding of cadherin-based mechanobiology. Trends Cell Biol. 25, 803–814. https://doi.org/10.1016/J.TCB.2015.09.008.

15. Leckband, D.E., le Duc, Q., Wang, N., and de Rooij, J. (2011). Mechanotransduction at cadherin-mediated adhesions. Curr. Opin. Cell Biol. 23, 523–530. https://doi.org/10.1016/J.CEB.2011.08.003.

16. Bays, J.L., Campbell, H.K., Heidema, C., Sebbagh, M., and Demali, K.A. (2017). Linking E-cadherin mechanotransduction to cell metabolism through force-mediated activation of AMPK. Nat. Cell Biol. 19, 724–731. https://doi.org/10.1038/ncb3537.

17. Labernadie, A., Kato, T., Brugués, A., Serra-Picamal, X., Derzsi, S., Arwert, E., Weston, A., González-Tarragó, V., Elosegui-Artola, A., Albertazzi, L., et al. (2017). A mechanically active heterotypic E-cadherin/N-cadherin adhesion enables fibroblasts to drive cancer cell invasion. Nat. Cell Biol. 19, 224–237. https://doi.org/10.1038/ncb3478.

18. To, S.K.Y., Mak, A.S.C., Eva Fung, Y.M., Che, C.-M., Li, S.-S., Deng, W., Ru, B., Zhang, J., and Wong, A.S.T. (2017). β-catenin downregulates Dicer to promote ovarian cancer metastasis. Oncogene 36, 5927–5938. https://doi.org/10.1038/onc.2017.185.

19. To, S.K.Y., Tang, M.K.S., Tong, Y., Zhang, J., Chan, K.K.L., Ip, P.P.C., Shi, J., and Wong, A.S.T. (2022). A selective β−catenin-metadherin/CEACAM1-CCL3 axis mediates metastatic heterogeneity upon tumor–macrophage interaction. Adv. Sci. 9, 2103230. https://doi.org/10.1002/ADVS.202103230.

20. Huang, L.P., Yu, Y.H., Sheng, C., and Wang, S.H. (2012). Up-regulation of cadherin 17 and down-regulation of homeodomain protein CDX2 correlate with tumor progression and unfavorable prognosis in epithelial ovarian cancer. Int. J. Gynecol. Cancer 22, 1170–1176. https://doi.org/10.1097/IGC.0B013E318261D89C.

21. Köbel, M., Kalloger, S.E., Boyd, N., McKinney, S., Mehl, E., Palmer, C., Leung, S., Bowen, N.J., Ionescu, D.N., Rajput, A., et al. (2008). Ovarian Carcinoma Subtypes Are Different Diseases: Implications for Biomarker Studies. PLoS Med. 5, 1749–1760. https://doi.org/10.1371/JOURNAL.PMED.0050232.

22. Patel, I.S., Madan, P., Getsios, S., Bertrand, M.A., and MacCalman, C.D. (2003). Cadherin switching in ovarian cancer progression. Int. J. Cancer 106, 172–177. https://doi.org/10.1002/IJC.11086.

23. Bauer, K., Gosau, M., Reinders, J., Oefner, P., Reichert, T.E., and Bauer, R. (2013). Presenilin 1/γ-secretase modulates P-cadherin processing and influences cell adhesion in oral squamous cell carcinoma cell lines. Carcinogenesis 34, 2622–2628. https://doi.org/10.1093/CARCIN/BGT211.

24. Barry, A.K., Tabdili, H., Muhamed, I., Wu, J., Shashikanth, N., Gomez, G.A., Yap, A.S., Gottardi, C.J., De Rooij, J., Wang, N., and Leckband, D.E. (2014). α-Catenin cytomechanics - role in cadherin-dependent adhesion and mechanotransduction. J. Cell Sci. 127, 1779–1791. https://doi.org/10.1242/JCS.139014/-/DC1.

25. Halvorson, D.L., and McCune, S.A. (1984). Inhibition of fatty acid synthesis in isolated adipocytes by 5-(tetradecyloxy)-2-furoic acid. Lipids 19, 851–856. https://doi.org/10.1007/BF02534514.

26. Yang, J., and Stack, M.S. (2020). Lipid regulatory proteins as potential therapeutic targets for ovarian cancer in obese women. Cancers 12, 3469–3525. https://doi.org/10.3390/CANCERS12113469.

27. Bertolio, R., Napoletano, F., Mano, M., Maurer-Stroh, S., Fantuz, M., Zannini, A., Bicciato, S., Sorrentino, G., and Del Sal, G. (2019). Sterol regulatory element binding protein 1 couples mechanical cues and lipid metabolism. Nat. Commun. 10, 1326–1411. https://doi.org/10.1038/s41467-019-09152-7.

28. Cheung, L.W.T., Leung, P.C.K., and Wong, A.S.T. (2010). Cadherin switching and activation of p120 catenin signaling are mediators of gonadotropin-releasing hormone to promote tumor cell migration and invasion in ovarian cancer. Oncogene 29, 2427–2440. https://doi.org/10.1038/onc.2009.523.

29. Sodi, V.L., Bacigalupa, Z.A., Ferrer, C.M., Lee, J.V., Gocal, W.A., Mukhopadhyay, D., Wellen, K.E., Ivan, M., and Reginato, M.J. (2018). Nutrient sensor O-GlcNAc transferase controls cancer lipid metabolism via SREBP-1 regulation. Oncogene 37, 924–934. https://doi.org/10.1038/ONC.2017.395.

30. Tan, W., Jiang, P., Zhang, W., Hu, Z., Lin, S., Chen, L., Li, Y., Peng, C., Li, Z., Sun, A., et al. (2021). Posttranscriptional regulation of de novo lipogenesis by glucose-induced O-GlcNAcylation. Mol. Cell 81, 1890–1904.e7. https://doi.org/10.1016/J.MOLCEL.2021.02.009.

31. Penque, B.A., Hoggatt, A.M., Herring, B.P., and Elmendorf, J.S. (2013). Hexosamine biosynthesis impairs insulin action via a cholesterolgenic response. Mol. Endocrinol. 27, 536–547. https://doi.org/10.1210/ME.2012-1213.

32. Contreras-Baeza, Y., Sandoval, P.Y., Alarcón, R., Galaz, A., Cortés-Molina, F., Alegría, K., Baeza-Lehnert, F., Arce-Molina, R., Guequén, A., Flores, C.A., et al. (2019). Monocarboxylate transporter 4 (MCT4) is a high affinity transporter capable of exporting lactate in high-lactate microenvironments. J. Biol. Chem. 294, 20135–20147. https://doi.org/10.1074/JBC.RA119.009093.

33. Doherty, J.R., and Cleveland, J.L. (2013). Targeting lactate metabolism for cancer therapeutics. J. Clin. Invest. 123, 3685–3692. https://doi.org/10.1172/JCI69741.

34. Corbet, C., Bastien, E., Draoui, N., Doix, B., Mignion, L., Jordan, B.F., Marchand, A., Vanherck, J.C., Chaltin, P., Schakman, O., et al. (2018). Interruption of lactate uptake by inhibiting mitochondrial pyruvate transport unravels direct antitumor and radiosensitizing effects. Nat. Commun. 9, 1208–1211. https://doi.org/10.1038/s41467-018-03525-0.

35. Chen, J., Ellert-Miklaszewska, A., Garofalo, S., Dey, A.K., Tang, J., Jiang, Y., Clément, F., Marche, P.N., Liu, X., Kaminska, B., et al. (2021). Synthesis and use of an amphiphilic dendrimer for siRNA delivery into primary immune cells. Nat. Protoc. 16, 327–351. https://doi.org/10.1038/s41596-020-00418-9.

36. Liu, X., Zhou, J., Yu, T., Chen, C., Cheng, Q., Sengupta, K., Huang, Y., Li, H., Liu, C., Wang, Y., et al. (2014). Adaptive amphiphilic dendrimer-based nanoassemblies as robust and versatile siRNA delivery systems. Angew. Chem. Int. Ed. Engl. 53, 11822–11827. https://doi.org/10.1002/ANIE.201406764.

37. Silva, A., Antunes, B., Batista, A., Pinto-Ribeiro, F., Baltazar, F., and Afonso, J. (2021). In vivo anticancer activity of AZD3965: A systematic review. Molecules 27, 181. https://doi.org/10.3390/MOLECULES27010181.

38. Vieira, A.F., and Paredes, J. (2015). P-cadherin and the journey to cancer metastasis. Mol. Cancer 14, 178–212. https://doi.org/10.1186/S12943-015-0448-4.

39. Kayahashi, K., Mizumoto, Y., Matsuoka, A., Obata, T., Iwadare, J., Nakamura, M., Daikoku, T., and Fujiwara, H. (2021). Mucinous, endometrioid, and serous ovarian cancers with peritoneal dissemination are potent candidates for P-cadherin targeted therapy: a retrospective cohort study. BMC Cancer 21, 32. https://doi.org/10.1186/S12885-020-07737-W.

40. Sun, L., Hu, H., Peng, L., Zhou, Z., Zhao, X., Pan, J., Sun, L., Yang, Z., and Ran, Y. (2011). P-cadherin promotes liver metastasis and is associated with poor prognosis in colon cancer. Am. J. Pathol. 179, 380–390. https://doi.org/10.1016/J.AJPATH.2011.03.046.

41. Zhang, C.C., Yan, Z., Zhang, Q., Kuszpit, K., Zasadny, K., Qiu, M., Painter, C.L., Wong, A., Kraynov, E., Arango, M.E., et al. (2010). PF-03732010: a fully human monoclonal antibody against P-cadherin with antitumor and antimetastatic activity. Clin. Cancer Res. 16, 5177–5188. https://doi.org/10.1158/1078-0432.CCR-10-1343.

42. Sousa, B., Pereira, J., Marques, R., Grilo, L.F., Pereira, S.P., Sardão, V.A., Schmitt, F., Oliveira, P.J., and Paredes, J. (2020). P-cadherin induces anoikis-resistance of matrix-detached breast cancer cells by promoting pentose phosphate pathway and decreasing oxidative stress. Biochim. Biophys. Acta, Mol. Basis Dis. 1866, 165964. https://doi.org/10.1016/J.BBADIS.2020.165964.

43. Sousa, B., Ribeiro, A.S., Nobre, A.R., Lopes, N., Martins, D., Pinheiro, C., Vieira, A.F., Albergaria, A., Gerhard, R., Schmitt, F., et al. (2014). The basal epithelial marker P-cadherin associates with breast cancer cell populations harboring a glycolytic and acid-resistant phenotype. BMC Cancer 14, 734–813. https://doi.org/10.1186/1471-2407-14-734.

44. Si, M., Wang, Q., Li, Y., Lin, H., Luo, D., Zhao, W., Dou, X., Liu, J., Zhang, H., Huang, Y., et al. (2019). Inhibition of hyperglycolysis in mesothelial cells prevents peritoneal fibrosis. Sci. Transl. Med. 11, eaav5341. https://doi.org/10.1126/SCITRANSLMED.AAV5341.

45. Bays, J.L., Peng, X., Tolbert, C.E., Guilluy, C., Angell, A.E., Pan, Y., Superfine, R., Burridge, K., and DeMali, K.A. (2014). Vinculin phosphorylation differentially regulates mechanotransduction at cell-cell and cell-matrix adhesions. J. Cell Biol. 205, 251–263. https://doi.org/10.1083/JCB.201309092.

46. Cheung, L.W.T., Mak, A.S.C., Cheung, A.N.Y., Ngan, H.Y.S., Leung, P.C.K., and Wong, A.S.T. (2011). P-cadherin cooperates with insulin-like growth factor-1 receptor to promote metastatic signaling of gonadotropin-releasing hormone in ovarian cancer via p120 catenin. Oncogene 30, 2964–2974. https://doi.org/10.1038/ONC.2011.7.

47. Lysne, D., Johns, J., Walker, A., Ecker, R., Fowler, C., and Lawson, K.R. (2014). P-cadherin potentiates ligand-dependent EGFR and IGF-1R signaling in dysplastic and malignant oral keratinocytes. Oncol. Rep. 32, 2541–2548. https://doi.org/10.3892/OR.2014.3545.

48. Smith, T.M., Gilliland, K., Clawson, G.A., and Thiboutot, D. (2008). IGF-1 induces SREBP-1 expression and lipogenesis in SEB-1 sebocytes via activation of the phosphoinositide 3-kinase/Akt pathway. J. Invest. Dermatol. *128*, 1286–1293. https://doi.org/10.1038/sj.jid.5701155.

49. Guo, D., Bell, E.H., Mischel, P., and Chakravarti, A. (2014). Targeting SREBP-1-driven lipid metabolism to treat cancer. Curr. Pharmaceut. Des. *20*, 2619–2626. https://doi.org/10.2174/13816128113199990486.

50. Röhrig, F., and Schulze, A. (2016). The multifaceted roles of fatty acid synthesis in cancer. Nat. Rev. Cancer *16*, 732–749. https://doi.org/10.1038/nrc.2016.89.

51. Gansler, T.S., Hardman, W., Hunt, D.A., Schaffel, S., and Hennigar, R.A. (1997). Increased expression of fatty acid synthase (OA-519) in ovarian neoplasms predicts shorter survival. Hum. Pathol. *28*, 686–692. https://doi.org/10.1016/S0046-8177(97)90177-5.

52. Chen, R.R., Yung, M.M.H., Xuan, Y., Zhan, S., Leung, L.L., Liang, R.R., Leung, T.H.Y., Yang, H., Xu, D., Sharma, R., et al. (2019). Targeting of lipid metabolism with a metabolic inhibitor cocktail eradicates peritoneal metastases in ovarian cancer cells. Commun. Biol. *2*, 281–315. https://doi.org/10.1038/s42003-019-0508-1.

53. Corn, K.C., Windham, M.A., and Rafat, M. (2020). Lipids in the tumor microenvironment: From cancer progression to treatment. Prog. Lipid Res. *80*, 101055. https://doi.org/10.1016/J.PLIPRES.2020.101055.

54. Yoon, H., and Lee, S. (2022). Fatty acid metabolism in ovarian cancer: Therapeutic implications. Int. J. Mol. Sci. *23*, 2170. https://doi.org/10.3390/IJMS23042170.

55. Nagarajan, S.R., Butler, L.M., and Hoy, A.J. (2021). The diversity and breadth of cancer cell fatty acid metabolism. Cancer Metabol. *9*, 2–28. https://doi.org/10.1186/S40170-020-00237-2.

56. Mukherjee, A., Bilecz, A.J., and Lengyel, E. (2022). The adipocyte microenvironment and cancer. Cancer Metastasis Rev. *41*, 575–587. https://doi.org/10.1007/S10555-022-10059-X.

57. Scaglia, N., Tyekucheva, S., Zadra, G., Photopoulos, C., and Loda, M. (2014). De novo fatty acid synthesis at the mitotic exit is required to complete cellular division. Cell Cycle *13*, 859–868. https://doi.org/10.4161/CC.27767.

58. Rowland, L.A., Guilherme, A., Henriques, F., DiMarzio, C., Munroe, S., Wetoska, N., Kelly, M., Reddig, K., Hendricks, G., Pan, M., et al. (2023). De novo lipogenesis fuels adipocyte autophagosome and lysosome membrane dynamics. Nat. Commun. *14*, 1362–1414. https://doi.org/10.1038/s41467-023-37016-8.

59. Li, J., Condello, S., Thomes-Pepin, J., Ma, X., Xia, Y., Hurley, T.D., Matei, D., and Cheng, J.X. (2017). Lipid Desaturation Is a Metabolic Marker and Therapeutic Target of Ovarian Cancer Stem Cells. Cell Stem Cell *20*, 303–314.e5. https://doi.org/10.1016/J.STEM.2016.11.004.

60. Hsiao, W.Y., and Guertin, D.A. (2019). De novo lipogenesis as a source of second Messengers in adipocytes. Curr. Diabetes Rep. *19*, 138. https://doi.org/10.1007/S11892-019-1264-9.

61. Gu, J., Zhou, J., Chen, Q., Xu, X., Gao, J., Li, X., Shao, Q., Zhou, B., Zhou, H., Wei, S., et al. (2022). Tumor metabolite lactate promotes tumorigenesis by modulating MOESIN lactylation and enhancing TGF-β signaling in regulatory T cells. Cell Rep. *39*, 110986. https://doi.org/10.1016/J.CELREP.2022.110986.

62. Battista, M.J., Goetze, K., Schmidt, M., Cotarelo, C., Weyer-Elberich, V., Hasenburg, A., Mueller-Klieser, W., and Walenta, S. (2016). Feasibility of induced metabolic bioluminescence imaging in advanced ovarian cancer patients: first results of a pilot study. J. Cancer Res. Clin. Oncol. *142*, 1909–1916. https://doi.org/10.1007/S00432-016-2200-X.

63. Chen, H., Wang, L., Beretov, J., Hao, J., Xiao, W., and Li, Y. (2010). Co-expression of CD147/EMMPRIN with monocarboxylate transporters and multiple drug resistance proteins is associated with epithelial ovarian cancer progression. Clin. Exp. Metastasis *27*, 557–569. https://doi.org/10.1007/S10585-010-9345-9.

64. Usui, A., Ko, S.Y., Barengo, N., and Naora, H. (2014). P-cadherin promotes ovarian cancer dissemination through tumor cell aggregation and tumor-peritoneum interactions. Mol. Cancer Res. *12*, 504–513. https://doi.org/10.1158/1541-7786.MCR-13-0489.

65. Klymenko, Y., Kim, O., Loughran, E., Yang, J., Lombard, R., Alber, M., and Stack, M.S. (2017). Cadherin composition and multicellular aggregate invasion in organotypic models of epithelial ovarian cancer intraperitoneal metastasis. Oncogene *36*, 5840–5851. https://doi.org/10.1038/ONC.2017.171.

66. Trillsch, F., Kuerti, S., Eulenburg, C., Burandt, E., Woelber, L., Prieske, K., Eylmann, K., Oliveira-Ferrer, L., Milde-Langosch, K., and Mahner, S. (2016). E-Cadherin fragments as potential mediators for peritoneal metastasis in advanced epithelial ovarian cancer. Br. J. Cancer *114*, 213–220. https://doi.org/10.1038/bjc.2015.436.

67. Bartolomé, R.A., Robles, J., Martin-Regalado, Á., Pintado-Berninches, L., Burdiel, M., Jaén, M., Aizpurúa, C., Imbaud, J.I., and Casal, J.I. (2021). CDH6-activated αIIbβ3 crosstalks with α2β1 to trigger cellular adhesion and invasion in metastatic ovarian and renal cancers. Mol. Oncol. *15*, 1849–1865. https://doi.org/10.1002/1878-0261.12947.

68. Lam, S.S.N., Ip, C.K.M., Mak, A.S.C., and Wong, A.S.T. (2016). A novel p70 S6 kinase-microRNA biogenesis axis mediates multicellular spheroid formation in ovarian cancer progression. Oncotarget *7*, 38064–38077. https://doi.org/10.18632/ONCOTARGET.9345.

69. Bankhead, P., Loughrey, M.B., Fernández, J.A., Dombrowski, Y., McArt, D.G., Dunne, P.D., McQuaid, S., Gray, R.T., Murray, L.J., Coleman, H.G., et al. (2017). QuPath: Open source software for digital pathology image analysis. Sci. Rep. *7*, 1–7. https://doi.org/10.1038/s41598-017-17204-5.

70. Luo, W., Friedman, M.S., Shedden, K., Hankenson, K.D., and Woolf, P.J. (2009). GAGE: Generally applicable gene set enrichment for pathway analysis. BMC Bioinf. *10*, 161–217. https://doi.org/10.1186/1471-2105-10-161.

71. Yung, S., Li, F.K., and Chan, T.M. (2006). Peritoneal mesothelial cell culture and biology. Perit. Dial. Int. *26*, 162–193. https://doi.org/10.1177/089686080602600207.

72. Chan, R.W.S., Mak, A.S.C., Yeung, W.S.B., Lee, K.F., Cheung, A.N.Y., Ngan, H.Y.S., and Wong, A.S.T. (2013). Human female reproductive tract epithelial cell culture. Methods Mol. Biol. *945*, 347–363. https://doi.org/10.1007/978-1-62703-125-7_21.

73. Liu, L., MacKenzie, K.R., Putluri, N., Maletić-Savatić, M., and Bellen, H.J. (2017). The glia-neuron lactate shuttle and elevated ROS promote lipid synthesis in neurons and lipid droplet accumulation in glia via APOE/D. Cell Metabol. *26*, 719–737.e6. https://doi.org/10.1016/J.CMET.2017.08.024.

STAR★METHODS

KEY RESOURCES TABLE

REAGENT or RESOURCE	SOURCE	IDENTIFIER
Antibodies		
P-cadherin	BD Biosciences	Cat #610227, RRID:AB_2077667
E-cadherin	CST	Cat #3195, RRID:AB_2291471
N-cadherin	CST	Cat #13116, RRID:AB_2687616
Cadherin-6	CST	Cat #48111, RRID:AB_2799334
Cadherin-17	CST	Cat #85724, RRID:AB_3669027
FASN	CST	Cat #3180, RRID:AB_2100796
Lipin 1	CST	Cat #14906, RRID:AB_2798644
SREBP1	Santa Cruz	Cat #sc-13551, RRID:AB_628282
β-actin	Sigma	Cat #A5316, AB_476743
P120ctn	CST	Cat #59854, RRID:AB_2799575
Rac	CST	Cat #2465, RRID:AB_2176152
Cdc42	CST	Cat #2462; RRID:AB_2078085
GAPDH	CST	Cat #2118, RRID:AB_561053
P-cadherin	Abcam	Cat #ab242060, RRID: AB_2889265
Ki67	CST	Cat #9027, RRID:AB_2636984
P-cadherin monoclonal antibody (NCC-CAD-299)	Thermo Fisher scientific	Cat #13-5800, RRID:AB_2533023
Anti-mouse IgG (H + L)-HRP Conjugate	Bio-Rad	Cat #1706516, RRID:AB_11125547
Anti-rabbit IgG (H + L)-HRP Conjugate	Bio-Rad	Cat #1706515, RRID:AB_11125142
Biological samples		
Human peritoneal mesothelial cells (HPMC)	Healthy donors	N/A
Normal human ovarian surface epithelial cells	Healthy donors	N/A
Ovarian cancer tumor sections	Patients	N/A
Chemicals, peptides, and recombinant proteins		
siLentFect Lipid Reagent for RNAi	Bio-Rad	Cat #1703360
Lipofectamine 2000	Thermo Fisher Scientific	Cat #11668027
AR-C155858	MedChemExpress	Cat #HY-13248
TOFA (5-(tetradecyloxy)-2-furoic acid)	Abcam	Cat #ab141578
CellTracker Blue CMAC Dye	Invitrogen	Cat #C2110
CellTracker Green CMFDA	Invitrogen	Cat #C7025
[U^{13}C] D-glucose	Cambridge Isotope Laboratories	Cat #CLM-1396-1
[13C3] sodium lactate	Cambridge Isotope Laboratories	Cat #CLM-1579-N
Human P-cadherin/Fc chimera protein	R&D systems	Cat #861-PC
Recombinant Human IgG1 Fc Protein, CF	R&D systems	Cat #110-HG
Critical commercial assays		
Lipid Staining Kit	BioVision	Cat #K580-24
L-Lactate Assay Kit	Abcam	Cat #ab65331
Rabbit specific HRP/DAB Detection IHC Kit	Abcam	Cat #ab64261
Active Rac1 Detection Kit	CST	Cat #8815
Active Cdc42 Dectection kit	CST	Cat #8819
Deposited data		
RNAseq analysis of HM cells with NS or P-cadherin siRNA [dataset]	This paper	GSA-Human: HRA004687

(Continued on next page)

Continued

REAGENT or RESOURCE	SOURCE	IDENTIFIER
Experimental models: Cell lines		
HEYA8 HM	To et al.[18] and To et al.[19]	N/A
HEYA8 NM	To et al.[18] and To et al.[19]	N/A
OVSAHO	JCRB	Cat #JCRB1046
MeT5A	ATCC	Cat #CRL-9444
Experimental models: Organisms/strains		
NOD/SCID/IL2rγnull (NSG) mice	Charles River Laboratories	Cat #614
Oligonucleotides		
ACAT2 forward primer 5′-CCTGTGGTCATCGTCTCGGC-3′	IDT	N/A
ACAT2 reverse primer 5′-AAGCCAAGTGAGGAGCCTTG-3′	IDT	N/A
ACLY forward primer 5′-AAGGGCATCGTGAGAGCAAT-3′	IDT	N/A
ACLY reverse primer 5′-TGGGACTGAATCTTGTGGCAT-3′	IDT	N/A
β-actin forward primer 5′-TCACCGAGGCCCCTCTGAACCCTA-3′	IDT	N/A
β-actin reverse primer 5′-GGCAGTAATCTCCTTCTGCATCCT-3′	IDT	N/A
CDH1 forward primer 5′-ACAGCCCCGCCTTATGATT-3′	IDT	N/A
CDH1 reverse primer 5′-TCGGACCGCTTCCTTCA-3′	IDT	N/A
CDH2 forward primer 5′-TGGGAATCCGACGAATGG-3′	IDT	N/A
CDH2 reverse primer 5′-GCAGATCGGACCGGATACTG-3′	IDT	N/A
CDH3 forward primer 5′-ACGAAGACACAAGAGAGATTGG-3′	IDT	N/A
CDH3 reverse primer 5′-AGCAACCACCCCATTGTAGG-3′	IDT	N/A
CDH6 forward primer 5′-TCAAGACAACAAAGACAACACG-3′	IDT	N/A
CDH6 reverse primer 5′-TCTCCACCACCTTCGTCGTT-3′	IDT	N/A
CDH17 forward primer 5′-ATGACAACCCTCCCAGGGC-3′	IDT	N/A
CDH17 reverse primer 5′-GACCCCGAAATAAGTGCTGA-3′	IDT	N/A
FASN forward primer 5′-CTGGCCTACACCCAGAGCTA-3′	IDT	N/A
FASN reverse primer 5′-CTCCATGTCCGTGAACTGCT-3′	IDT	N/A
FN1 forward primer 5′-AAGACAGACGAGCTTCCCCA-3′	IDT	N/A
FN1 reverse primer 5′-CTATGCCTTATGGGGGGTGGC-3′	IDT	N/A
Gpi forward primer 5′-GCGAGGCCAGAGTCCAATAA-3′	IDT	N/A

(Continued on next page)

Continued

REAGENT or RESOURCE	SOURCE	IDENTIFIER
Gpi reverse primer 5′-GACCAGCCTTCCCTGCTAAG-3′	IDT	N/A
GLUT1 forward primer 5′-GCAAGTCCTTTGAGATGCTGATCC-3′	IDT	N/A
GLUT1 reverse primer 5′-GCCGACTCTCTTCCTTCATATCC-3′	IDT	N/A
HK2 forward primer 5′-CCAGTTCATTCACATCATCAG-3′	IDT	N/A
HK2 reverse primer 5′-CTTACACGAGGTCACATAGC-3′	IDT	N/A
HSL forward primer 5′-TCAGTGTGCTCTCCAAGTGTGTC-3′	IDT	N/A
HSL reverse primer 5′-GCTATGGGCTCCGACATCTTC-3′	IDT	N/A
MAGL forward primer 5′-TTGCTGCGAAAGTGCTCAAC-3′	IDT	N/A
MAGL reverse primer 5′-ATTCAGCAGTTGGATGCCGA-3′	IDT	N/A
Perilipin1 forward primer 5′-GAAACAGCATCAGCGTTCCC-3′	IDT	N/A
Perilipin1 reverse primer 5′-ATGGTCTGCACGGTGTATCG-3′	IDT	N/A
PGK1 forward primer 5′-CTGTGCCAAATGGAACACGG-3′	IDT	N/A
PGK1 reverse primer 5′-AGTTGACTTAGGGGCTGTGC-3′	IDT	N/A
SLC16A1 forward primer 5′-TGGATGGAGAGGAAGCTTTCTAAT-3′	IDT	N/A
SLC16A1 reverse primer 5′-CACACCAGATTTTCCAGCTTTC-3′	IDT	N/A
SREBF1 forward primer 5′-ACAGTGACTTCCCTGGCCTAT-3′	IDT	N/A
SREBF1 reverse primer 5′-GCATGGACGGGTACATCTTCAA-3′	IDT	N/A
ON-TARGETplus CDH1 siRNA	Dharmacon	D-003877-07-0005
ON-TARGETplus CDH2 siRNA	Dharmacon	J-011605-06-0005
ON-TARGETplus CDH3 siRNA	Dharmacon	J-003823-12-0005
ON-TARGETplus CDH6 siRNA	Dharmacon	J-011991-07-0005
ON-TARGETplus CDH17 siRNA	Dharmacon	J-011829-06-0005
ON-TARGETplus OGT siRNA	Dharmacon	J-019111-08-0005
ON-TARGETplus SREBP1 siRNA	Dharmacon	J-006891-08-0005
ON-TARGETplus MCT4 siRNA	Dharmacon	J-005126-23-0005
ON-TARGETplus Non-targeting control siRNA	Dharmacon	D-001810-02-20
Recombinant DNA		
P-cadherin	Lam et al.[68]	N/A
Software and algorithms		
Prism 8.0	Graphpad	https://www.graphpad.com/
QuPath 0.4.4	Bankhead et al.[69]	https://qupath.github.io/
GAGE	Luo et al.[70]	http://sysbio.engin.umich.edu/~luow/downloads.php

EXPERIMENTAL MODEL AND STUDY PARTICIPANT DETAILS

Cell lines

HEYA8 HM and NM ovarian cancer cell sublines were constructed and maintained as previously described.[18,19] In brief, isogenic HM (highly metastatic) and NM (non-metastatic) cell lines were established by isolating migrated and non-migrated HEYA8 cell clones, respectively, from migration assay, and the differential metastatic properties were confirmed by orthotopic injection. HM and NM cells were maintained in RPMI 1640. MeT5A were maintained in Medium 199:MCDB105 (1:1). All culture medium were supplemented with 5% fetal bovine serum (FBS), 100 U/mL penicillin and 100 μg/mL streptomycin (Invitrogen).

Primary cell cultures and human patient samples

Primary human peritoneal mesothelial cells (HPMC) were isolated from dialysate effluent from peritoneal dialysis from patients with nonmalignant disorders as previously described.[71] The collection of PD fluid was approved by the Institutional Review Board of the University of Hong Kong/Hospital Authority Hong Kong West Cluster. HPMC were used within three passages to ensure genetic stability of the culture. Normal human ovarian surface epithelial (OSE) cells were derived from surface scrapings of normal ovaries from women with nonmalignant gynecological diseases as previously described.[72] OSE and HPMC were maintained in Medium 199:MCDB105 (1:1) supplemented with 5% fetal bovine serum, 100 U/mL penicillin and 100 μg/mL streptomycin (Invitrogen).

Formalin-fixed paraffin-embedded (FFPE) clinical samples of paired ovarian high-grade serous carcinoma and metastases were obtained from the pathology archives of Department of Pathology, University of Hong Kong, for immunohistochemical analyses. Clinicopathological information of patients were provided in Table S1. Primary tumor ascitic samples were obtained from 7 patients with high grade serous ovarian cancer (Stage III/IV). Ascitic cells were collected following centrifugation and removal of red blood cells. The use of these specimens was approved by the Institutional Ethical Review Board for Research on the use of human subjects at the University of Hong Kong.

Mice

Female NOD/SCID/IL2rγ^{null} (NSG) mice were purchased from Charles River Laboratories. HM, NM or transfected HM cells (1 × 10⁶) were intraperitoneally (i.p.) injected into NSG mice (n = 3 mice per group) and sacrificed after 3 weeks to focus on the early stages of metastatic dissemination and adhesion. For dendriplexes treatment, mice bearing intraperitoneally injected HM cells were intravenously injected with siNS-AmDM, siP-cad-AmDM, siMCT1-AmDM or siMCT4-AmDM for 3 weeks (siRNA: 1.0 mg/kg, N/P ratio = 5, twice a week). At sacrifice, the volume of ascites was measured and all visible (>0.1 cm) metastatic tumor nodules were counted. All mouse studies were performed according to the protocols approved by the University of Hong Kong Animal Care and Use Committee.

METHOD DETAILS

Transfection and inhibitor treatment

Transient transfection with siRNA oligos (Dharmacon) or overexpression plasmids were performed using siLentFect for RNAi (Bio-Rad) or Lipofectamine 2000 (Thermo Fisher Scientific), respectively. To establish cell lines with stable knockdown, cells were transduced with MISSION shRNA Lentiviral Transduction Particles (Sigma) according to the manufacturer's protocols. For MCT inhibition, cells were treated with 200 nM monocarboxylate transporter inhibitor AR-C155858 (MedChemExpress) for 24 h. For inhibition of acetyl-CoA carboxylase, cells were pretreated with TOFA (Abcam, 20 μM) for 2 h and then cocultured with MeT5A monolayer for 24 h. For inhibition of OGT, cells were treated with OSMI-1 (MedChemExpress, 10 μM) together with Fc- or P-cad/Fc-coated beads for 24 h. For inhibition of N-glycan biosynthesis and surface N-glycan removal, cells were treated with tunicamycin (MedChemExpress, 100 nM) or PNGase F (New England Biolabs) together with Fc- or P-cad/Fc-coated beads for 24 h.

Cell adhesion assay

Mesothelial cells were seeded on 96-well plates and cultured to form confluent monolayer. CMFDA (Invitrogen)-labeled cancer cells were then added to the monolayer at a concentration of 1×10⁴ cells per well and incubated at 37°C for 30 min. After gentle washing for three times with PBS, the plates were loaded on Cytation 1 (BioTek) for cell counting at the GFP channel. At least five microscopic fields of the adhered cells were quantified for each condition.

Single-cell force spectroscopy

Cancer-mesothelial cell rupture forces were measured using JPK NanoWizard II (Bio-AFM). MeT5A cells were seeded at a density of 10⁴ cells/well on the 30 mm glass bottom dish (MatTek) and cultured overnight. Cantilevers were coated with 0.1 μg/mL poly-D-lysine solution (Sigma) for 6 h, rinsed with water before calibration using the thermal noise method. For cell-cell rupture force measurement, single cancer cell was picked up onto the cantilever with contact for 5 s, after which cancer cell was brought to contact with single MeT5A cell (medium changed to FBS-free RPMI 1640) for 5 s, with approach/retraction velocities of 5 μm s⁻¹ and contact force of 2 nN. Force curves were collected and analyzed with JPK data processing software. For P-cadherin blocking group, HM and MeT5A

cells were pre-incubated with 10 μg/mL P-cadherin antibody (NCC-CAD-299) (Thermo Fisher Scientific) for 15 min, after which rupture forces were measured as stated above.

Western blot analysis

After SDS-PAGE, proteins were transferred to nitrocellulose membranes, which were blocked with 5% non-fat dry milk for 1 hand incubated with primary antibodies for 1 h to overnight. The membranes were washed thrice and incubated with appropriate secondary antibodies conjugated with HRP (Bio-rad; 1:3,000). Bands were detected by Western-Lightning Plus Enhanced Chemiluminescence (PerkinElmer), and their intensities were determined by densitometry using ImageJ. P-cadherin (BD Biosciences, #610227), E-cadherin (CST, #3195), N-cadherin (CST, #13116), Cadherin-6 (CST, #48111), Cadherin-17 (CST, #85724), FASN (CST, #3180), Lipin 1 (CST, #14906), SREBP1 (Santa Cruz, #sc-13551), and β-actin (Sigma, #A5316) were used.

Detection of active Rac1, Cdc42

Active Rac1 and Cdc42 was assessed by Active RAC1 detection kit and Active Cdc42 detection kit (Cell Signaling Technology) according to manufacturer's instruction.

Fluorescence staining

Cells (2×10^5) were seeded in confocal dish 24 h before the indicated treatment. Cells were fixed with ice-cold methanol for 20 min and permeabilized with 1% Triton X-100 for 30 min. Cells were washed with PBS and blocked with 5% BSA in PBS for 20 min, followed by incubation with primary antibody (1:100) overnight or phalloidin for 1 h. After washing with PBS, cells were incubated with dye-conjugated secondary antibody (1:100) for 1 h. Stained cells were mounted with Prolong antifade mountant with DAPI (Invitrogen).

Oil red O (ORO) staining

ORO staining was carried out using Lipid Staining Kit (BioVision). Briefly, cells were treated as indicated and fixed with Formalin (10%) for 30 min before staining with ORO in 60% isopropanol for 15 min. Confocal imaging was used to capture the Oil red O signals. Only signals overlaying with green fluorescence (from tumor cells labeled with CellTracker Green) were measured. At least five microscopic fields were quantified for each condition. Acquisition settings remained the same in all groups of fluorescent images.

Glucose uptake assay

Cells were inoculated in a 6-well plate in 5% FBS supplemented culture medium. After the indicated treatment for 24 h, medium was changed to glucose-free medium with 100 μg/mL 2-NBDG. Cells were incubated for 45 min and washed twice with ice-cold PBS, before loading on Cytation 1. More than 3 technical replicates were analyzed for cell counting by ImageJ.

L-lactate measurement

The L-lactate levels of cells or culture medium were measured by L-Lactate Assay Kit (Abcam). Cells were collected by centrifugation and resuspended in 100 μL lactate assay buffer, which were then homogenized and centrifuged to collect supernatant for L-lactate assay. The culture medium was measured directly according to the manufacturer's instructions.

Seahorse extracellular flux analysis

Mitochondrial and glycolysis bioenergetics were investigated using Seahorse Extracellular Flux analyzer (Agilent). Cells were treated with siRNA for 24 h and reseeded onto 24-well XF plates for another 24 h before bioenergetics analysis. Growth medium was then changed with XF base medium (pH, 7.4) containing 25 mM glucose, 1 mM sodium pyruvate, and 2 mM glutamine for mitochondrial bioenergetics assay, or 2 mM glutamine (Sigma) for glycolysis bioenergetics assay. Oxygen consumption rate (OCR) or extracellular acidic rate (ECAR) profiles were generated after the injection of 1.5 μM oligomycin, 3 μM FCCP and 1.2 μM rotenone+1.2 μM antimycin A for OCR, or 15 mM Glucose, 1.5 μM oligomycin, 75 mM 2-DG for ECAR every 24 min. The average of four baseline rates and up to five test rates were used for data analysis.

Proliferation assay

HM cells labeled with CMFDA were inoculated on the mesothelial monolayer or alone in RPMI 1640 supplemented with 5% FBS, and monitored every 24 h for 4 days. More than 3 technical replicates were analyzed for cell counting by ImageJ.

$^{13}C_6$-glucose and lactate competition assay

The lactate competition assay was modified from reported method.[73] Briefly, mesothelial monolayer was first placed in RPMI 1640 (Gibco) containing 25 mM [U^{13}C]-glucose (Cambridge Isotope Laboratories) for 24 h. The monolayer was then washed with glucose-free RPMI 1640 and labeled with CellTracker Blue CMAC Dye (Invitrogen) for 45 min before coculture with CellTracker Green CMFDA Dye (Invitrogen)-labeled HM cells. The cells were further cultured in RPMI-1640 supplemented with 25 mM [U^{13}C]-glucose in the absence or presence of 11 mM L-lactate (Sigma).

^{13}C-metabolic flux analysis

^{13}C-lactate tracing was performed in mice which were first i.p. injected with NM or HM cells. After 3 weeks, during which the metastatic tumors had formed, mice were fasted for 3 h before receiving i.p. injection of 10 mM ^{13}C$_3$ sodium lactate (Cambridge Isotope Laboratories). After 3 h, mice were sacrificed and the metastatic tumors were harvested for targeted lipidomics analysis. For ^{13}C-glucose flux analysis, MeT5A seeded in 100 mm dish were cultured in glucose-free medium containing 25 mM [U^{13}C$_6$]-glucose for 24 h. CellTracker Green CMFDA Dye (Invitrogen)-labeled HM cells transfected with siP-cad or siNS were subsequently added for coculture. After 24 h, cells were collected and HM cells were isolated by fluorescence-activated cell sorting. Cells were extracted and subjected to GC-MS/MS analysis through an Agilent DB-23 capillary column and acquired in an Agilent 7890B GC-Agilent 7010 Triple Quadrapole Mass Spectrometer system (Santa Clara, USA). For fatty acids flux analysis, fatty acids were determined after transesterification by methanol and concentrated hydrochloric acid (35%, w/w). For determination of PEP and pyruvate, extracted samples by methanol/water (80%, v/v) were derivatized with methoxylamine hydrochloride and MSTFA with 1% TMCS. Metabolite fragment ions of monoisotopic mass (denoted M + 0) and mass isotopologues of higher mass were quantified in SIM mode. A scan range from m/z 50–500 was used to acquire mass spectra in SCAN mode. Data analysis was performed using the Agilent MassHunter Workstation Quantitative Analysis Software. Relative fractions of mass isotopologues were calculated from the peak areas of corresponding SIM ions. Raw data acquisition was performed with assistance of the University of Hong Kong Li Ka Shing Faculty of Medicine Center for PanorOmic Sciences Proteomics and Metabolomics Core.

Cell sorting

After cocultured for 24 h, fluorescent-labeled cells were sorted by BD FACSMelody cell sorter, and collected in RPMI 1640 supplemented with 5% FBS at 4°C.

Treatment with Fc- or P-cadherin/Fc-coated beads

Magnetic beads were coated with recombinant human P-cadherin/Fc chimera protein or recombinant human IgG1 Fc protein (R&D systems) according to manufacturer's instructions. Briefly, 1.5 mg Dynabeads Protein A (Invitrogen) were incubated with 50 μL Fc or P-cad/Fc protein (100 μg/mL) in 200 μL PBS with 0.1% Tween 20 for 10 min at room temperature. Beads were collected using magnet to remove unbound protein and washed once with PBS with 0.1% Tween 20, and then resuspended in 200 μL PBS. Cells seeded in a 6-well plate were treated with 15 μL of coated beads per well. For the treatment of cancer cells, medium was supplemented with 11 mM L-lactate (Sigma). The coated beads were stored at 4°C and used within one week.

RNA extraction and reverse-transcription PCR analysis

Total RNA was first extracted using Trizol reagent (Ambion) and then reverse-transcribed to cDNA using M-MLV reverse transcriptase (Invitrogen). PCR was performed with a set of primers as listed in key resources table.

RNA sequencing and data analysis

RNA was extracted from HM cells were transfected with NS or P-cadherin siRNA and sent to BGI for transcriptomic RNA sequencing (*n* = 2). Data have been deposited in the Genome Sequence Archive (China National Center for Bioinformation) which are publicly accessible at https://ngdc.cncb.ac.cn/gsa-human (GSA-Human: HRA004687). Dysregulated pathways were identified with Generally Applicable Gene-set Enrichment (GAGE).

siRNA dendriplexes formation

AmDM (MW = 3838 g/mol, 16 amine end groups) were dissolved in distilled H$_2$O and stocked in 500 μM. To prepare the siRNA dendriplexes, dendrimer and siRNA were first diluted separately in OPTI-MEM (Invitrogen) and incubated at room temperature for 5 min (siRNA dosage: 1 mg/kg, N/P ratio: 5). Dendrimer and siRNA were mixed and incubated at room temperature for 20 min before treatment.

Immunohistochemistry

FFPE sections from patient or mice tumors were deparaffinized with xylene and rehydrated in graded ethanol. After blocking and heat-induced antigen retrieval using citrate buffer, the specimens were separately incubated with primary antibody (FASN (#3180, CST, 1; 100), P-cadherin (ab242060, Abcam, 1:1000), Ki67 (#9027, CST, 1:1000) overnight at 4°C. The slides were further processed using rabbit specific HRP/DAB (ABC) detection IHC kit according to the manufacturer's protocol (Abcam). Slides were subsequently scanned on an Akoya Vectra Polaris scanner scanning at ×20 magnification and semi-quantitative analysis of cytoplasmic FASN, membrane P-cadherin and nuclear Ki-67 expression was performed using QuPath 0.4.4 software. Five fields per specimen with the strongest marker expression were selected for cell detection and tumor cell classification. Followed by single cell detection, staining intensity (0, negative; 1, weak; 2, medium and 3, strong) and percentage of positive tumor cells were assessed based on pre-defined arbitrary signal intensity. Gene expression was graded with an H-score as previously reported, which is calculated by multiplying the percentage of positive cells (0–100) by the intensity (0–3). Data are expressed as median H-score.

Detection of active Rac1, Cdc42

Active Rac1 and Cdc42 was assessed by Active RAC1 detection kit and Active Cdc42 detection kit (Cell Signaling Technology) according to manufacturer's instruction.

QUANTIFICATION AND STATISTICAL ANALYSIS

GraphPad Prism 8 was used for plotting and analysis of data. All experiments were carried out in duplicates or triplicates and repeated at least two times. All data are presented as mean ± SD unless otherwise indicated. Data derived from two groups were compared by unpaired Student's t test. Data derived from more than two groups were compared by one-way ANOVA followed by a Tukey's test. Paired sample t test is used for comparing expression of markers in paired patient specimens. Differences were considered statistically significant when the p value was less than 0.05. 'n' in this study represents either the number of biological replicates for *in vitro* experiments or number of mice for *in vivo* experiments.